D.6

ATTEL

PERFORMANCE-BASED APPROACHES FOR HIGH STRENGTH TUBULAR COLUMNS AND CONNECTIONS UNDER EARTHQUAKE AND FIRE LOADINGS

Deliverable 6:
"Design Guidelines and proposal for EC3, EC4 and EC8"

Contributors:
University of Thessaly
University of Liège
Centro Sviluppo Materiali
Stahlbau Pichler
University of Trento

21/03/2012

Table of Contents

This document constitutes the final deliverable from European RFCS project ATTEL. Design guidelines and optimization of the design of structural configurations such as base joints, HSS columns and composite beam-to-column joints are proposed taking into account the experimental and numerical results obtained within the project.

Design guidelines for steel buildings with high-strength steel CHS columns

In this design guidelines for buildings for which high-strength steel can give an economical solution are presented; the reference buildings 1 and 2 (see WP2) in the present project are examples of buildings for areas of low and high seismicity respectively. For these building, static, seismic and fire actions are considered; design guidelines from global structural analysis to the verification of structural elements (e.g. column bases, tubular columns and beam-to-column joints) are proposed.

It should be noted that the present guidelines (a) are in-line with the current EN 1993 design practice and (b) propose some possible amendments for high-strength steel(HSS) tubular CHS members. The proposed amendments are based on the imperfection and residual stress measurements, the test data and the numerical results obtained within the present research project, for the seamless CHS tubes described in the previous sections of this report. A list of publications is offered, which support the proposed guidelines.

1. Structural solution

1.1 Building structures in low-seismicity areas

A cost-efficiency study has been carried out within the present project [11]; from the latter, the following conclusions can be drawn for the definition of a structural solution where HSS can have an economical interest.

1.1.1 Columns

(1) For isolated steel columns: stocky columns are recommended and the interest of using HSS decreases when the eccentricity of the axial load increases.

(2) For columns in frames: a global schematic view on the interest of using high-strength steel in comparison with normal steel (NS)/S355 is presented in Table 1. Possibilities for using high-strength steel are quite large when considering braced/non-sway frames using steel columns. On the other hand, there is no benefit in using high-strength steel for steel columns in sway frames, if compared to frames using normal steel. Moreover, for frames using composite columns, very few possibilities for using HSS can be identified.

Table1. Summary of the conclusions of the analysis

Frame type	Column type	
	Steel column	Composite column
Braced/non-sway frames	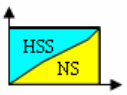 Many possibilities for HSS	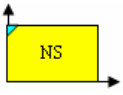 Very few possibilities for HSS
Un-braced/sway frames	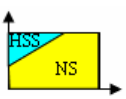 There are possibilities for HSS	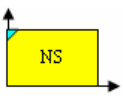 Very few possibilities for HSS

(3) In fire condition: almost no economic interest exists in using columns made of high-strength steel without protection, in both steel and composite columns. If a protection is used, the use of high-strength steel may lead to benefits as it is the case for normal temperature.

Accordingly, in the next section, mainly guidelines for braced/non-sway frames will be recommended/derived.

1.1.2. Slabs and joints

The following solutions for slabs and joints are suggested for a braced/non-sway frame using high-strength steel tubes for the columns.

(1) Using composite floors with a concrete/composite slab connected to the steel beams through shear connectors in order to activate a composite action at the joint level

(2) Using configurations for column bases and beam-to-column joints as shown in Fig.1. The column bases are formed by one full end plate welded to the column and anchored in the concrete block by four anchor bolts. With respect to the beam-to-column joint configuration: one through plate is welded to the column, on this plate two horizontal plates (each side of the column) are attached by fillet welds. The lower flanges of steel beam are connected to the horizontal plates using bolts.

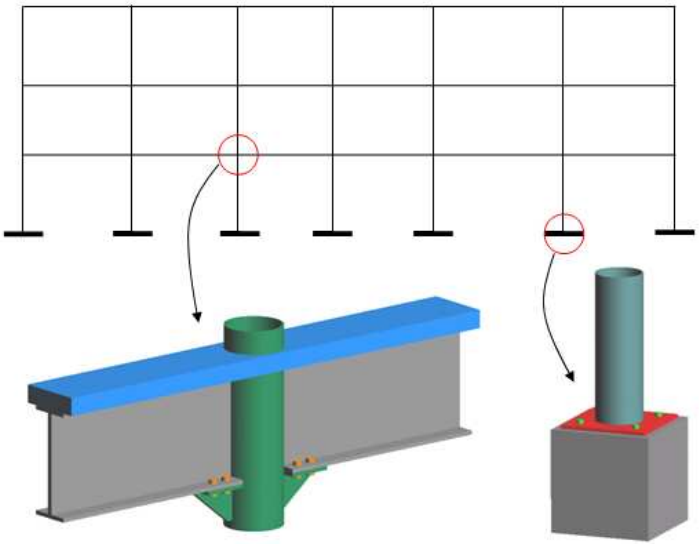

Fig.1. Suggested beam-to-column joint and column base for frames subjected to static loads

1.2 Building structures in areas of significant seismicity

Building structures subjected to medium-high seismic loadings are usually realized using moment resisting frames only along one direction. This is customarily done to contain the cost of joints designed satisfying capacity design rules. A cost-efficiency study was carried out considering the 2D moment resisting frame, see Fig.2, of the prototype structure. In detail both the design and the economic evaluation of the frame were realized considering four different solutions of circular columns: i) hollow columns with mild steel, NS S355; ii) composite columns with mild steel, NS S355; iii) hollow columns with high strength steel, HSS S590; iv) composite columns with high strength steel, HSS S590.

1.2.1 Columns

The analysis conducted on the different solutions showed the advantage of using high-strength steel S590 with respect to the mild steel NS S355. In fact the use of columns endowed with high-strength steel with the same geometry of the columns realized with mild steel complies with capacity design rules. This does not require the increase of the column sections with economic savings of about 15%.

1.2.2. Beam- to- column and column-base joints

The solutions suggested for beam-to-column and base-column joints with columns with HSS follow:

(1) beam-to column joints designed as rigid and full strength joints and realized by bolted connection, as showed in Fig. 1. A vertical through plate and two horizontal plates were welded to the column in order to bolt the beams by means of cover plates. The use of composite columns exhibits better strength and stiffness than simple connections to the tube face. In fact, this connection avoids all possible phenomena of large instability in the wall around the joint region.

(2) Two solutions for column-base joints: i) a standard solution with base plate, anchor bolts and vertical stiffeners; ii) an innovative solution with a column embedded in the concrete foundation. Both the plate welded around the column and the four anchor bolts are used for column erection purposes.

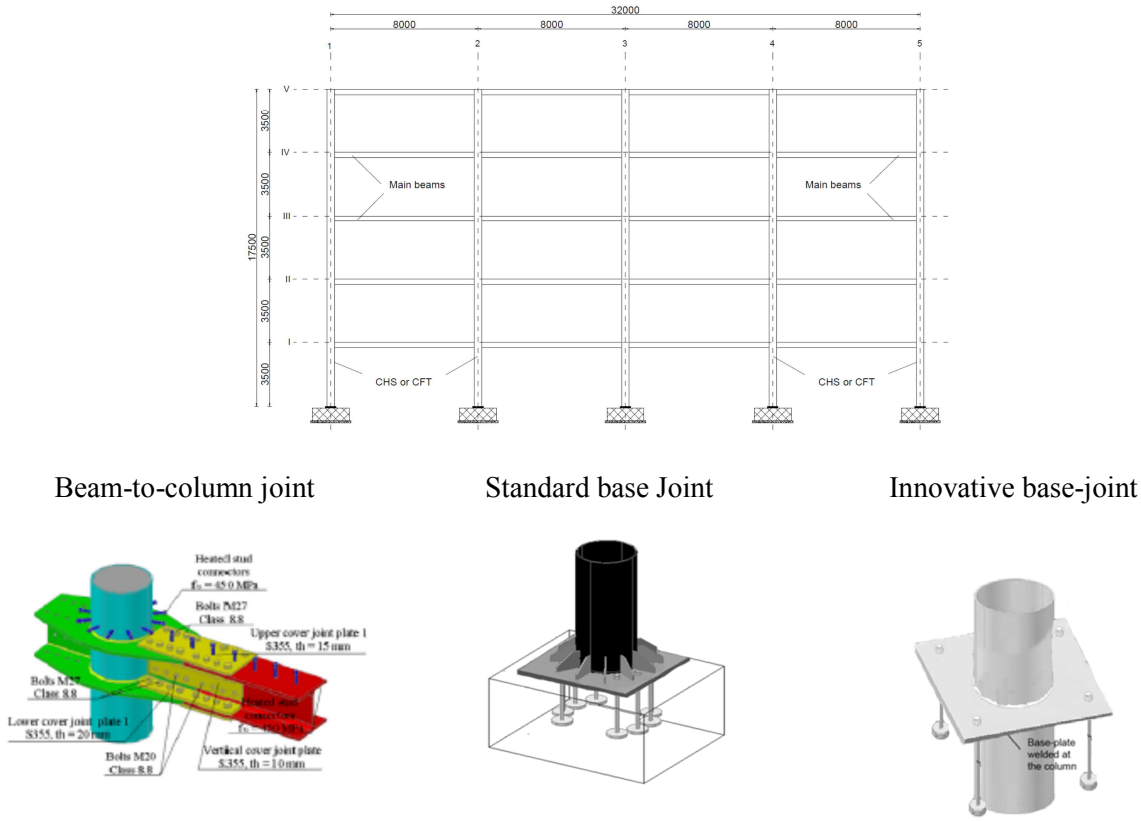

Fig.2. Suggested beam-to-column joint and column bases, standard and innovative, for MRF subjected to seismic loads

2. Global analysis of frames

2.1 Building structures in areas of low seismicity

(1) During the construction phase: the behaviour of beam-to-column joints as illustrated in Fig. 1 must be considered as hinges. The column base behaviour may be considered as semi-rigid and partial strength. Globally, elastic analysis for simple steel frames should be adopted.

(2) During the exploitation phase: both beam-to-column joints and column base can be considered as semi-rigid and partial strength joints. Globally, elastic/plastic analyses for semi-continuous composite frames could be applied.

2.2 Building structures in areas of significant seismicity

The behaviour of both beam-to-column and column-base joints, showed in Fig 2, could be assumed as rigid and full strength both during the erection and exploitation phases. In particular, the configuration of column-base joints is the same in both phases; even though beam-to column joints lack the presence of the composite action during erection, they are rigid and full strength anyway. In this phase, in fact, the strength is assured by the slip resistance owing to preloaded bolts used in connections. Both the joints and the structures can be assumed to belong to a medium ductility class during structural analysis under seismic loading. These properties were confirmed by test results.

3. Design of high-strength steel CHS columns

3.1 Design of high-strength steel CHS columns at normal temperature

The design procedure follows the general framework of EN 1993 parts 1-1 [2] and 1-6 [3]. The rules in EN1993-1-1 (Sections 6.3.1-6.3.3) can be used, following the existing classification (see Appendix C),

shown in *Table 2*. This design procedure results in safe, yet conservative predictions. However, some amendments to these rules are proposed, to account for the above conservativeness for high-strength steel CHS seamless members, similar to the tubes considered in the present work [4] [5], with wrinkling imperfection amplitudes not exceeding 2.6% of the tube thickness (see Appendix C).

Table 2. CHS member classification according to EN 1993-1-1

Class	Class limits	Class limits in terms of shell slenderness $\bar{\lambda}$
1	$D/t \le 50\varepsilon^2$	$\bar{\lambda} \le \bar{\lambda}_1 = 0.278$
2	$50\varepsilon^2 \le D/t \le 70\varepsilon^2$	$\bar{\lambda}_1 = 0.278 < \bar{\lambda} \le \bar{\lambda}_2 = 0.329$
3	$70\varepsilon^2 \le D/t \le 90\varepsilon^2$	$\bar{\lambda}_2 = 0.329 < \bar{\lambda} \le \bar{\lambda}_3 = 0.373$
4	$D/t \ge 90\varepsilon^2$	$\bar{\lambda} > \bar{\lambda}_3 = 0.373$

3.1.1 Cross-sectional strength for axial loading

Shell slenderness is defined as follows [3]:

$$\bar{\lambda}=\sqrt{\frac{\sigma_y}{\sigma_e}} \tag{1}$$

where σ_y is the yield stress and

$$\sigma_e=0.605C_xE\frac{t}{r} \tag{2}$$

For member slenderness $\bar{\lambda} \le 0.60$, the axial compression load is calculated as follows:

$$N_{Rk}=\sigma_y A \quad \text{if} \quad \bar{\lambda} \le \bar{\lambda}_3=0.373 \tag{3}$$

$$N_{Rk} = \sigma_y A\left(1-\beta_\alpha \frac{\bar{\lambda}-\bar{\lambda}_3}{\bar{\lambda}_\alpha-\bar{\lambda}_3}\right) \quad \text{if} \quad \bar{\lambda} > \bar{\lambda}_3 \tag{4}$$

where $\beta_a=0.133$, $\bar{\lambda}_\alpha=0.6$ and $\bar{\lambda}_3=0.373$.

The above equations are valid for values of shell slenderness $\bar{\lambda}$ less than 0.60, and are shown in Fig.3b, together with test data and numerical results [4].

3.1.2 Cross-sectional strength for bending loading

The value of shell slenderness $\bar{\lambda}$ is obtained from the equation (1). The bending strength of the cross section is calculated as follows:

$$M_{Rk}=M_p=\sigma_y W_{pl} \quad \text{if} \quad \bar{\lambda} \le \bar{\lambda}_2=0.329 \tag{5}$$

$$M_{Rk} = M_p\left(1-\beta_b \frac{\bar{\lambda}-\bar{\lambda}_2}{\bar{\lambda}_b-\bar{\lambda}_2}\right) \quad \text{if} \quad \bar{\lambda} > \bar{\lambda}_2 \tag{6}$$

where $\beta_b=0.22$, $\bar{\lambda}_b=0.5$ and $\bar{\lambda}_2=0.329$

The above equations are valid for values of shell slenderness $\bar{\lambda}$ less than 0.60, and are shown in Fig.3a, together with test data and numerical results [4].

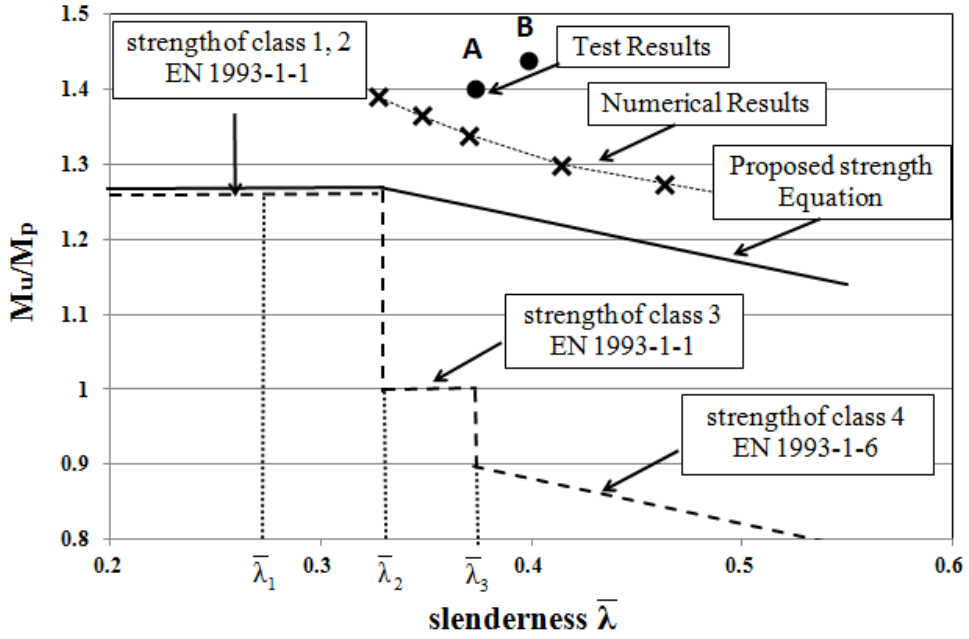

Fig.3a Bending capacity versus shell slenderness [4].

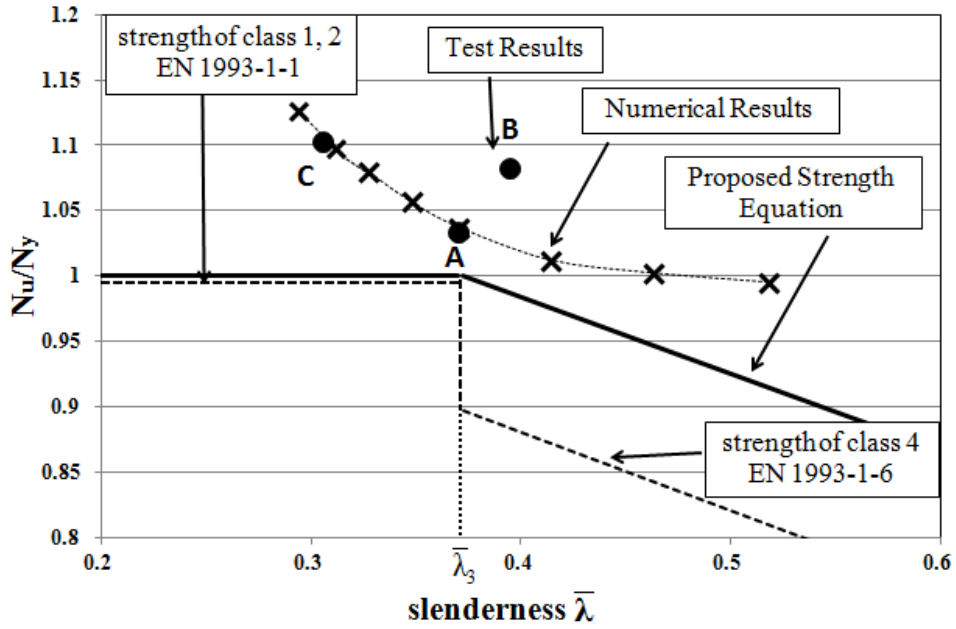

Fig.3b Axial load capacity versus shell slenderness [4].

3.1.3 Strength of CHS columns

The strength of tubular members under combined loading of axial load and bending is calculated from the interaction curve proposed by EN-1993-1-1 paragraph 6.3 [2]:

$$\frac{N_{Ed}}{\chi N_{Rk}} + k\frac{M_{Ed}}{M_{Rk}} = 1 \qquad (7)$$

where M_{Ed} and N_{Ed} are the acting axial and bending loads, and N_{Rk}, M_{Rk} represent the cross sectional axial and bending strength respectively (defined above). The k factor is a coefficient that depends on axial load and the shape of the bending moment diagram along the members, defined in Annex A or B of EN1993-1-1. The buckling reduction factor χ depends on column slenderness

$$\lambda = \sqrt{\frac{N_{Rk}}{N_e}} \tag{8}$$

where N_e is the elastic buckling load of the tubular column. Note that the above definition of λ accounts for CHS sections which may not reach the full plastic axial load. Finally, it is recommended to use curve α_0, for the reduction factor $\chi(\lambda)$ as defined in EN1993-1-1 [2]. More FE results are reported in Appendix D.

3.2 Design of high-strength steel CHS columns at elevated temperature

The following remarks should be kept in mind for the design of these columns in fire conditions (elevated temperature).

(1) The design of circular columns made of HSS under fire action should be based on Eurocodes 3, part 1-2 [6], and Eurocode 4, part 1-2 [8] for steel and composite columns respectively.

(2) The use of stress-strain relationship at elevated temperature initially developed for carbon steel provided results that well reproduced the prediction of vertical displacements, if compared to the experimental results. Also, for the circular filled tube column, the fire resistance predicted with the Eurocode rules was in good agreement with that found experimentally.

(3) However, the fire resistance of the tested steel columns was overestimated using the material model of Eurocode 3, part 1-2 [6]; the so-obtained predictions are significantly influenced by the considered initial imperfection. To obtain a fire resistance in line with the experimental evidence, the imperfection shall not be taken less than L/200, which is not in line with the recommended initial imperfection for such elements. This aspect should be investigated in more details, what constitutes a perspective to the present project.

4. Design of column base subjected to combined bending moment and axial force

4.1. Static column-bases under static loading

4.1.1. Introduction

(1) Three parts should be considered at the level of the column base:

- column (steel tube);
- tube-to-plate weld;
- end plate in bending, anchor bolts in tension and concrete in compression.

(2) The bending moment-axial resistance interaction zone for the whole column base is defined from the ones of the joint components (Fig.4). The way to characterise these components is given here below.

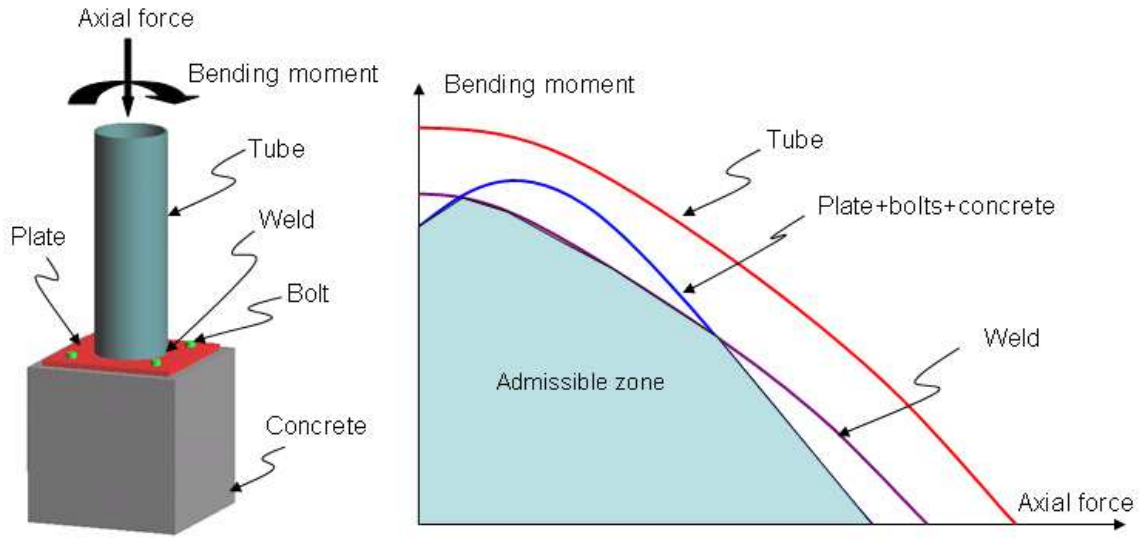

Fig.4. Design guidelines for column bases

4.1.2. Tube and tube-to-plate weld

Resistance of the components "tube" and "tube-to-plate weld" can be calculated using Eurocode 3, part 1.1 [2]. The bending moment-axial resistance interaction curves for these components can be easily established knowing their geometrical and material characteristics.

4.1.3. Plate in bending, bolts in tension and concrete in compression

(1) The applied moment (M_{Ed}) and axial force (N_{Ed}) are equilibrium by the "concrete in compression" (f_i) and "plate in bending, bolts in tension" (F_t) components (Fig.5). The interaction curve of bending moment and axial force (Fig.4) can be established using two equilibrium equations for the bending moment and axial force (detail can be found in Appendix A).

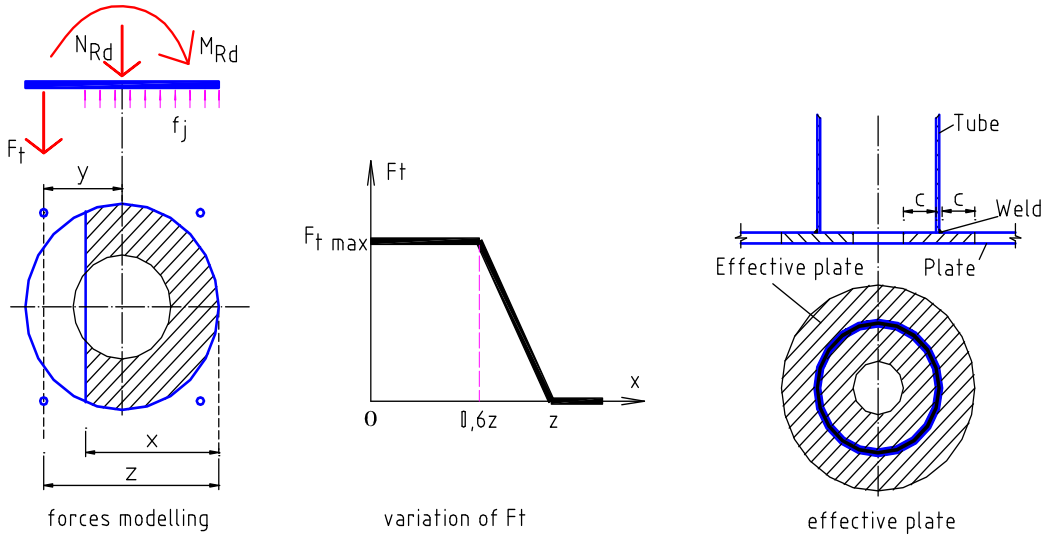

Fig.5. Column base - Assembly of plate, anchor bolts and concrete block components

(2) "Concrete in compression" component: a concentration effect has to be considered to compute the resistance of the concrete in compressing by using the "concentration ratio". Moreover, to characterise this component, the flexibility of the end plate should also be taken into account through the definition of an effective rigid plate, see Fig.5. The details to characterise this component can be found in Appendix A.

(3) "Plate in bending, bolts in tension" component: this component is modelled by a force (F_t) at the bolt position (Fig.5). This force varies according to the width of the compression zone, and their relation proposed in [9] can be applied here, as illustrated in Fig.5. The maximal value of F_t ($F_{t,max}$) may be calculated by Eq.(9) as follows:

$$F_{t,\max} = (M_{p,\min} - bm_p)/w \qquad (9)$$

with $M_{p,min}$ is the minimum value of M_{pi} (i=1-7) given in Table 3; b and m_p are the width and the unit plastic moment of the end plate, respectively. In Table 3: all geometric quantities are defined on Fig.6; B is the yield force per bolt; the coefficients α_1, α_2, α_3 and α_4 are given in Appendix A, depend on the geometries of the end plate and the bolt positions.

Noting that M_{pi} in Table 3 is furnished from a limit analysis of the "plate in bending and bolts in tension" component on the rigid foundation (Fig.6). Kinematical approach is applied with seven (7) licit mechanisms is in considering (Fig.7). It should be noted that: the calculation of the two local mechanisms (Figs.7a and 7b) can be found in Eurocode 3, part 1.8 [7]. The length of the yield lines in three mechanisms (Figs.7c, 7d and 7g) are fixed (equal to the flange width) so that the corresponding capacities of these modes can be directly computed. On the other hand, the methods for the calculation of the two mechanisms (Figs.7e and 7f) have been developed within this project and are reported Appendix A.

Table 3: determination of M_{pi}

Yield pattern	Failure mode	Plastic moment (M_{pi})
Circular (Fig.7a)	Mode 1– thin plate	$M_{p1} = [8\pi w' + b]m_p$
Circular (Fig.7b)	Mode 1 – thin plate	$M_{p2} = [4(\pi + e/n')w' + b]m_p$
Noncircular (Fig.7c)	Mode 1– thin plate	$M_{p3} = 2(d'/s' + 1)bm_p$
Noncircular (Fig.7d)	Mode 2 – intermediate plate	$M_{p4} = \left(\frac{d'}{e_1 + s'} + 2\right)bm_p + \frac{2e_1 d'}{e_1 + s'}B$
Noncircular (Fig.7e)	Mode 1- thin plate	$M_{p5} = \alpha_1 bm_p$ (*)
Noncircular (Fig.7f)	Mode 2 – intermediate plate	$M_{p6} = (\alpha_2 m_p + 2\alpha_3 B)b$ (*)
Noncircular (Fig.7g)	Mode 3 – thick plate	$M_{p7} = bm_p + 2w'B$

$d' = d + 2*0.8*\sqrt{2}a$; $s' = s - 0.8\sqrt{2}a$; $w' = w + 0.8\sqrt{a}$; other symbols are defined on Fig.6.

(*): these values of M_{p5} and M_{p6} are calculated in taking into account the prying force (in the zone next to the tension bolts). If the prying force is not considered, the following value of moment is recommended to use instead of M_{p5} and M_{p6}: $M^* = \alpha_4 bm_p$. Noting that, in Eurocode 3, part 1-8 [7], the calculation without the prying force is recommended.

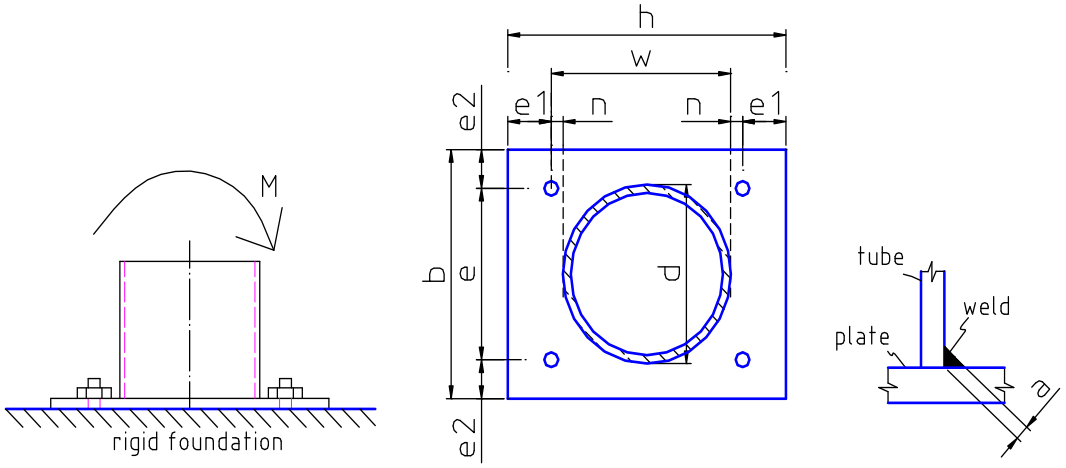

Fig.6: Column base – model for limit analysis of plate and bolts

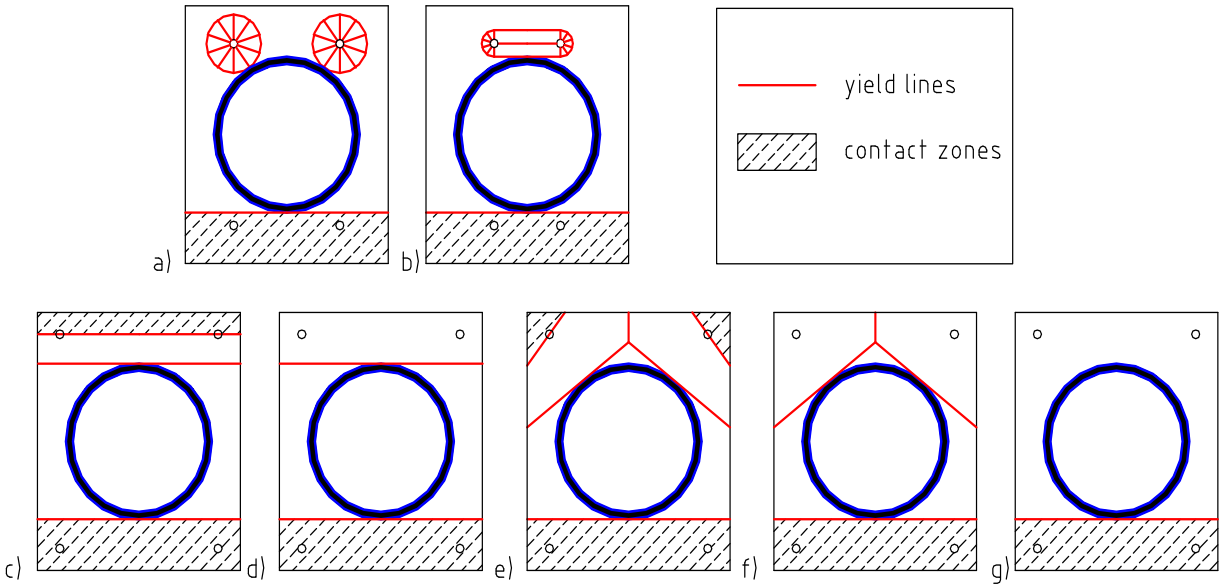

Fig.7: Column base - considered mechanisms for the end plate

4.2. In elevated temperature conditions (fire)

The design guidelines given for the column base at normal temperature can be used in case of fire loading; only material characteristics (yield strength and Young modulus) must be adapted according to the variation of temperature.

4.3. Additional guidelines on the design of seismic column-base joints

Both the standard and the innovative solution showed in Fig.2, can be designed coping with the capacity design rules suggested by EN1998-1-1 (2005). Along this line, the strength requested by EN1998-1-1 (2005) for foundation elements was calculated via the following formula:

$$E_{Fd} = E_{FG} + \gamma_{Rd} \cdot \Omega \cdot E_{FE},$$

considered in what follows.

4.3.1 Standard seismic column-base joints

The use of the above-mentioned formula permits to obtain a base joint characterized by adequate stiffness and strength to transfer the action of the column to the foundation. The proper design of stiffeners permits to locate the plastic hinge far from the weld between the column and the base plate, thus avoiding brittle failure. In fact, the response of this base-joint under cyclic tests exhibited a ductile behaviour without stiffness and strength degradation. The collapse of the joint was due to the anchor bolts after the activation of the plastic hinge associated with plastic rotations of about 45 mrad.

4.3.2 Innovative seismic column-base joints

The innovative seismic base joint realized by means of a column embedded in the foundation permits a cheap solution to be obtained, characterized by stiffness and strength higher than the standard solution. The behaviour of this base joint is like the one employed for pocket foundations. The only function for both, of the base plate and of the anchor bolts, is to permit the column to be vertically erected. This joint exhibited ductile behaviour characterized by large plastic rotation of about 45 mrad with brittle failure on weld between the column and the base plate, due to phenomena of local instability in the wall of the column. To avoid the brittle failure, it is possible to weld some stiffeners in order to govern the zone of instability from the weld of the column to the base plate. The design of this joint regarded only the foundation that can be designed according to the Strut & Tie mechanism proposed for prefabricated concrete constructions, according to EN 1992-1-1 (2005). In detail, both test results and numerical analyses by FE modelling with Abaqus indicate that three struts are present in the plinth. Fig shows both the geometry of the struts in the plinth obtained via numerical analysis and the distribution of compressive principal stresses.

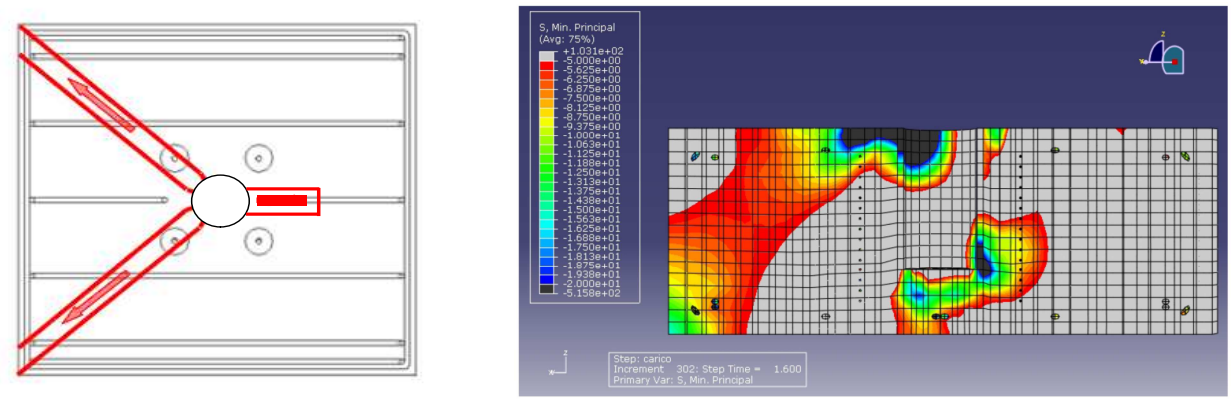

Fig.8. FE results relevant to the plinth of the innovative column-base joint: a) strut & tie mechanism; b) distribution of compressive principal stresses.

4.4. Guidelines on the design of seismic column bases made of HSS subjected to fire loading

The EN1993-1-2 (2005) and EN1994-1-2 (2005) are adequate codes to design under fire loading the typology of seismic column bases (standard -CB2- and innovative -CB3-) made of HSS tested in the project. In fact, the experimental evidence highlighted that the failure occurred in both specimens owing to the collapse of the column that lost its capacity to withstand the applied load because of the degradation of its mechanical properties with high temperatures. The parts constituting the joint between the foundation and the column did not undergo severe damage: in CB2 the bolts, the vertical stiffeners and the end plate were only slightly damaged whereas in CB3 no major damage was detected. The failure mode involving the column entailed a gradual loss of capacity till failure associated to a fire resistance between 81 and 87 minutes under the applied loads thanks also to the contribution of concrete in the steel tube.

From this viewpoint, the detailing of the joint shall be carefully designed. The rebars inside the tube that end in the foundation, as well as the tube itself in the case of CB3, shall be adequately drowned in the concrete base by providing a sufficient anchorage length. This is also valid for the anchor bolts. The presence of concrete in the tube and the joint detailing, that envisages continuity both of rebars (CB2) and of the tube (CB3), are reckoned the main factors for an enhanced fire resistance rather than the HSS tube itself.

5. Design of beam-to-column joints

5.1. Static beam-to-column joints

5.1.1. General

The bending moment-rotation curve of the joints can be defined by characterising the following components (Fig.9):

- longitudinal slap reinforcement in tension (K1 in Fig.9);
- bolts in shear (K2 in Fig.9);
- plate in bearing (K3 in Fig.9);
- through plate and column in diagonal compression (K4 in Fig.9);

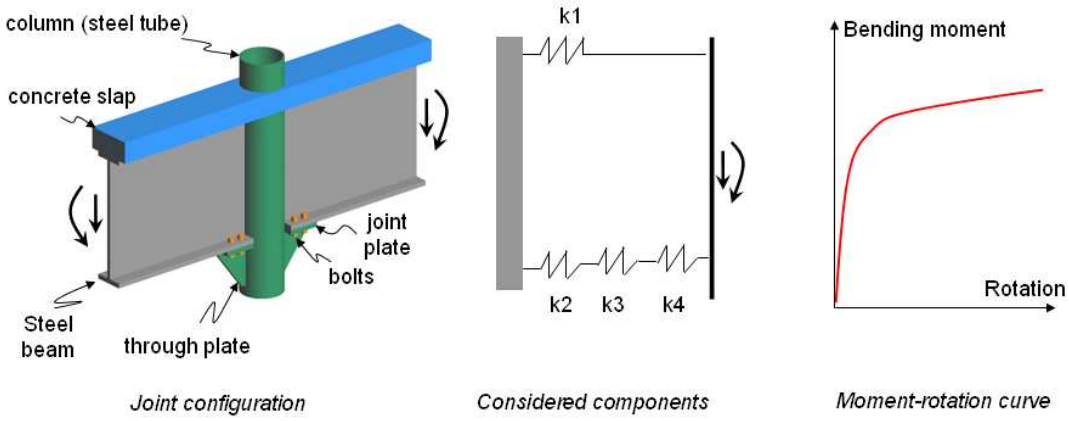

Fig.9. Proposed beam-to-column joint and components to be characterised

5.1.2. Longitudinal slap reinforcement in tension, bolts in shear and plate in bearing

The detail calculation for the characterization of the component "longitudinal slap reinforcement in tension" can found in [1], while the components "bolts in shear" and "plate in bearing" can be found in [7].

5.1.3. Through plate and column in diagonal compression

The method to characterise this component loaded as illustrated in Fig. 10 has been developed within the present project; the details are reported in Appendix B, some remarks are presented in the following. The through plate is devised into two parts, inside part (inside the column) and outside parts (outside the column), the buckling theory of plate is applied to study the strength of each part. The traditional formula of the elastic buckling is used while the plasticity and the initial imperfection are taken into account by a parameter that is determined from a numerical analysis (parametric study). Finally, the safety verification of the through plate may be performed by the following formula:

$$\begin{cases} \dfrac{V_{Ed}}{th} \le \kappa\mu_1 \dfrac{\pi^2 E}{12(1-\upsilon^2)}\left(\dfrac{t}{b}\right)^2 / \gamma_{M1}; \\ \dfrac{4F_{Ed}}{th} + \dfrac{4V_{Ed}b}{th^2} \le \mu_2 \dfrac{\pi^2 E}{12(1-\upsilon^2)}\left(\dfrac{t}{h}\right)^2 / \gamma_{M1}. \end{cases} ; \quad (10)$$

with V_{Ed} and F_{Ed} are the vertical and horizontal components of the applied load (Fig.10); E and υ are the Young modulus and Poisson ratio of the material, respectively; γ_{M1} is the partial factor according to EN1993-3-1 [2]; κ= 1.0 for the rectangular outside part and κ = 0.9 for the triangular outside part; μ_1 and μ_2 are given in Appendix B, depend on the load direction (α - ratio between the vertical and the horizontal loads), the column diameter (D), the plate dimensions (thickness (t), width (b), and height (h)), and the material characteristics; all geometries of the plate are defined on Fig.10.

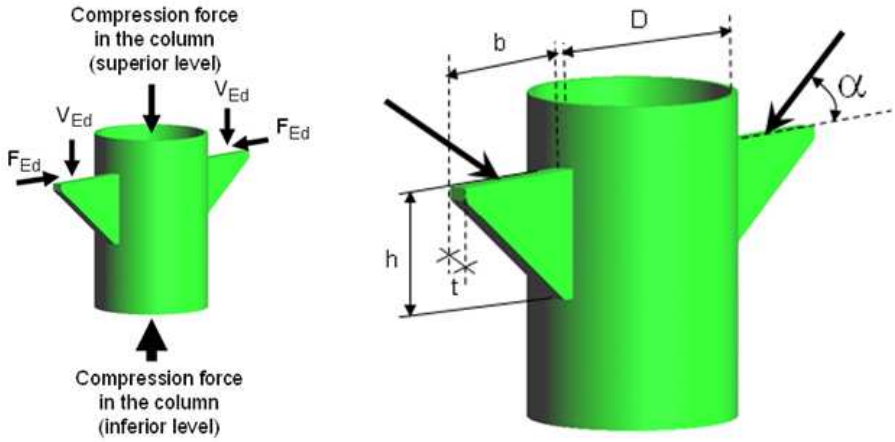

Fig.10. Beam-to-column joints - through plate component

5.1.4. In elevated temperature conditions (fire)

The remarks made in Section 4.4 remain valid.

5.2. Additional guidelines on the design of seismic beam-to-column joints

The innovative beam-to-column joint realized by bolted connections between the beam and weld plate at the column exhibit a ductile behaviour, see Fig. 2. The joint can be designed in agreement with EN1993-1-1 (2005), EN1994-1-1 (2005) and EN1998-1-1 (2005) respecting the concept of the capacity design with plastic hinge located on weak section between the end of the beam and the plate welded on the column. The design of beam-to-column joints with the shear connectors only on the upper flange of the beam permits to obtain a cheap solution. In agreement with the component method and test results, the innovative solution shows a ductile behaviour characterized by slip in bolted connections for high value of displacement and force, in agreement with the type of bolted connection, category B; please see EN1993-1-8 (2005).
The design by the component method requires the simulation of the joint by means of a series of different components. Each component was represented by an elastic spring characterised by a specific stiffness and strength, as highlighted in Figure . The appropriate coupling in parallel and series of these springs provides the global stiffness of the joint. As far as the global connection strength was concerned, different failure mechanisms were identified, the minimum value of failure loads being the design resistance of the connection. The components considered are reported in Table .

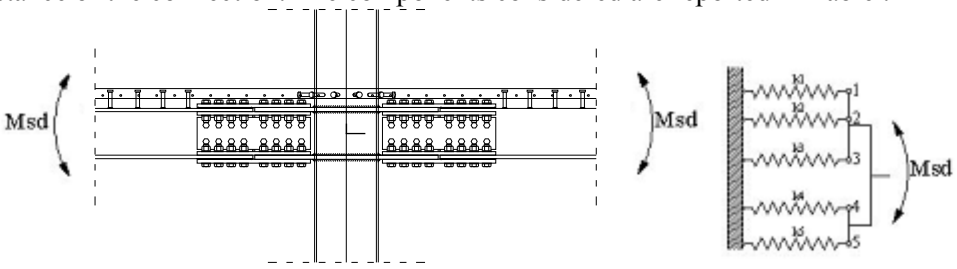

Figure 11. A steel-concrete composite bolted beam-to-column joint and its mechanical model.

The composite column was assumed to be infinitely rigid during the application of the component method. In greater detail, beam-to-column joints were rigid and full-strength joints. The joint overstrength can be guaranteed by the following relation

$$M_{j,Rd} \geq 1.1 \cdot \gamma_{ov} \cdot M_{b,pl,Rd}$$

where $M_{j,Rd}$ defines the resisting moment of the beam-to-column joint assumed to be full strength and $M_{b,pl,Rd}$ represents the resisting moment of the adjacent composite beam.

Table 4. Joint components relevant to sagging and hogging bending moment

Sagging Bending Moment	**Hogging Bending Moment**
Concrete slab in compression	Longitudinal rebars in tension
Upper horizontal plate in compression	Upper horizontal plate in tension
Vertical plate in bending	Vertical plate in bending
Lower horizontal plate in tension	Lower horizontal plate in compression

References

[1] Anderson D (ed). COST C1 - Composite steel-concrete joints in frames for buildings: Design provisions. Brussels – Luxembourg, 1999.

[2] Eurocode 3: Design of steel structures, Part 1-1: General rules and rules for buildings. EN 1993-1-1, Brussels, 2005.

[3] Eurocode 3: Design of steel structures - Part 1-6: Strength and Stability of Shell Structures. EN 1993-1-6, Brussels, 2007.

[4] Pappa, P., and Karamanos, S. A., *"Buckling of High-Strength Steel CHS Tubular Members under axial compression and bending,"* 14th International Symposium on Tubular Structures, Paper No. 104, London, UK, 2012.

[5] Pournara A.E., Karamanos S.A., Ferino J., Lucci A., "*Strength and stability of high-strength steel tubular beam-columns under compressive loading*," 14th International Symposium on Tubular Structures, Paper No. 103, London, UK, 2012.

[6] Eurocode 3: Design of steel structures, Part 1-2: General rules - Structural fire design. EN 1993-1-2, Brussels, 2004.

[7] Eurocode 3: Design of steel structures - Part 1-8: Design of joints. EN 1993-1-8, Brussels, 2003.

[8] Eurocode 4: Design of composite steel and concrete structures, Part 1-2: General rules - Structural fire design. EN 1994-1-1, Brussels, 2004.

[9] Guisse S, Vandegans D, Jaspart JP. Application of the component method to column bases – experimentation and development of a mechanical model for characterization. Research Centre of the Belgian Metalworking Industry, 1996.

[10] Eurocode 4: Design of composite steel and concrete structures, Part 1-1: General rules and rules for buildings. EN 1994-1-1, Brussels, 2004.

[11] Hoang VL et al. Field of application of high strength steel circular tubes for steel and composite columns from an economic point of view. Journal of Constructional Steel Research, (67):1001-1021, 2011.

Appendix A: Static column base

A1. Introduction

This appendix details Section 4.1.3, on:

- the assembly of the component (detail of the interaction equations);
- the calculation of the “concrete in compression” component;
- the calculation of the “end plate in bending, bolts in tension” component.

A2. Notices

Geometric dimensions of the column base are indicated on Fig.A1.

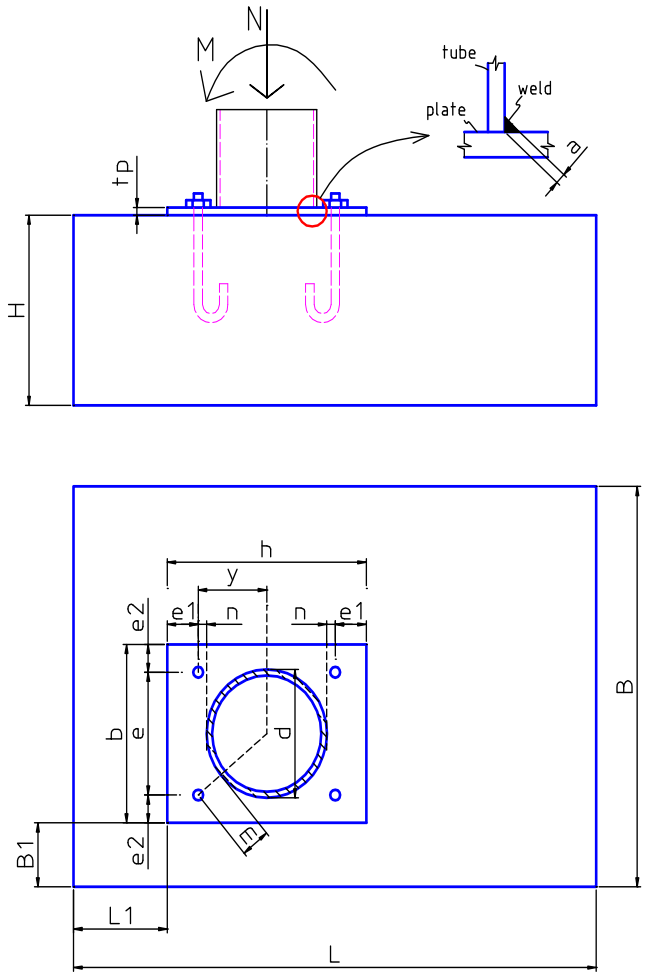

$$d' = d + 2*0.8*\sqrt{2}a \; ; \; s' = s - 0.8\sqrt{2}a$$

Fig.A1. Geometric dimensions of the static column base

A3. Assembly of the components (interaction equations)

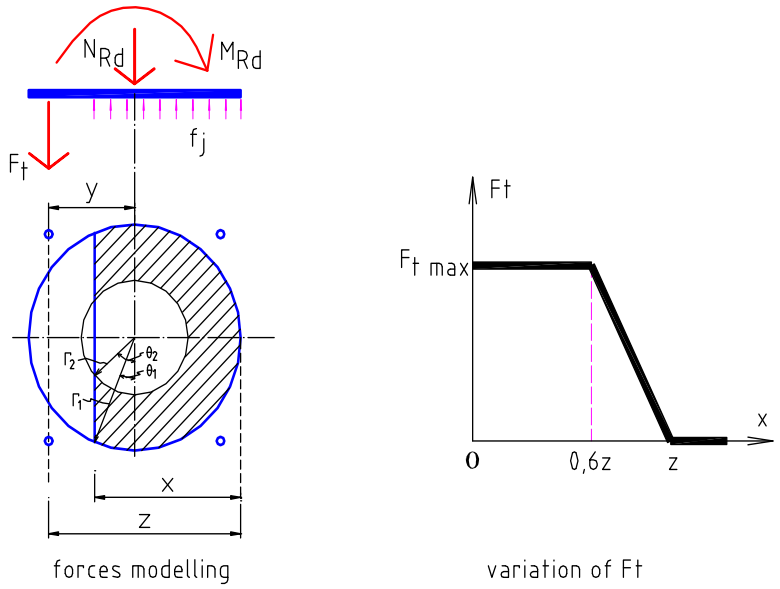

Fig.A2. Column base - Assembly of plate, anchor bolts and concrete block components

The applied moment (M_{Ed}) and axial force (N_{Ed}) are equilibrium by the "concrete in compression" (f_i) and "plate in bending, bolts in tension" (F_t) components (Fig.A2). The force F_t varies according to the width of the compression zone as the show on Fig.A2, this relation is proposed in [2]. How to obtain f_i (concrete in compression) and F_{tmax} (plate in bending, bolts intension) are presented in Section A.4 and A.5, respectively. When f_i and F_t are determined, the interaction curve of bending moment and axial force can be written as Eqs. (A1) and (A2):

$$N_{Rd} = A_c f_j - F_{t,x}; \tag{A1}$$

$$M_{Rd} = (S_1 - S_2) f_j + F_{t,x} y. \tag{A2}$$

with

$$A_c = A_{eff} - (A_1 - A_2)$$

$$A_{eff} = \pi(r_1^2 - r_2^2)$$

$$A_1 = r_1^2(\pi/2 - \theta_1 - \sin\theta_1 \cos\theta_1)$$

$$A_2 = r_2^2(\pi/2 - \theta_2 - \sin\theta_2 \cos\theta_2)$$

$$S_1 = \frac{2}{3} r_1^3 \cos^3\theta_1$$

$$S_2 = \frac{2}{3} r_2^3 \cos^3\theta_2$$

$$F_{t,x} = \begin{cases} 0 & \text{if} \quad x \geq z \\ 2.5F_t(z-x)/z & \text{if} \quad 0.6z \leq x < z \\ F_t & \text{if} \quad x < 0.6z \end{cases}$$

$$z = r_1 + y$$

$$\theta_2 = \begin{cases} \arctan \dfrac{r_1 \sin\theta_1}{\sqrt{r_2^2 - (r_1 \sin\theta_1)^2}} & \text{if} \quad r_2^2 - (r_1 \sin\theta_1)^2 > 0 \\ \pi/2 \quad \text{if} \quad r_2^2 - (r_1 \sin\theta_1)^2 \le 0 \end{cases};$$

Let θ_1 vary from $-\pi/2$ to $\pi/2$, using Eqs. (A1) and (A2), it is possible to depict the interaction curve (curve ABC on Fig.A3).

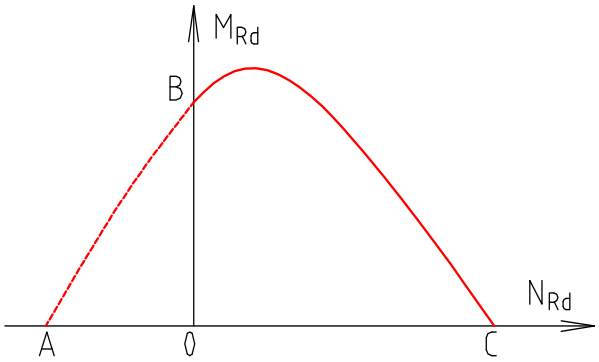

Fid.A3. Interaction curve for plate in bending, bolts in tension and concrete in compression

A4. "Concrete in compression" component [2]

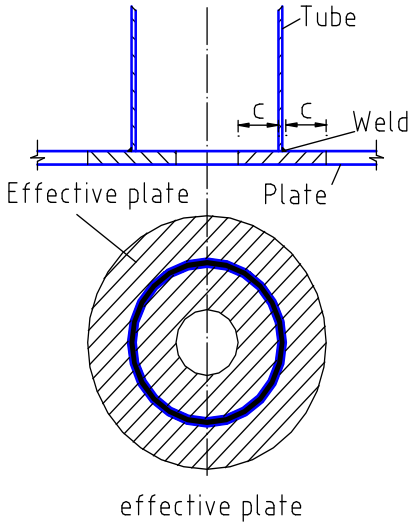

Fig.A4. Effective plate

Due to the volume effect, the strength of the concrete in compression should be multiplied by the "concentration ratio". On the other hand, due to the flexibility of the end plate, the concrete reaction applies only within a zone defined by an effective rigid plate, see Fig.A4.

The concentration ratio is calculated Eq.A3 as follow:

$$k_j = \sqrt{\frac{B_{eff} L_{eff}}{bh}} \tag{A3}$$

with B_{eff} and L_{eff} are the effective dimensions of the concrete block and they are determined by Eq.A4:

$$\begin{aligned} B_{eff} &= \min(b + 2B_1; 5b; h_p + H; 5L_{eff}) \ge b \\ L_{eff} &= \min(h + 2L_1; 5h; h_p + H; 5B_{eff}) \ge h \end{aligned} \tag{A4}$$

The admissible stress in the concrete block can reach the value, Eq.(A5):

$$f_j = \beta_j k_j \frac{f_{ck}}{\gamma_c} \tag{A5}$$

with $\beta_j = 2/3$; f_{ck} is the characteristic strength of the concrete in compression; γ_c is the partial safety factor for the concrete.

The equivalent rigid plate (Fig.A4) is a ring that is determined through the parameter c (Fig.A4) by Eq.A6:

$$c = t_p \sqrt{\frac{f_{yp}}{3 f_j \gamma_{M0}}} \tag{A6}$$

where t_p is the base plate thickness; f_{yp} is the yielded strength of the base plate; γ_{M0} is the partial safety factor for the steel.

A5. The "end plate in bending, bolts in tension" component

A5.1. Development

This component is developed by using limit analysis on the column base where rigid-plastic material concept is used for the end plate and the bolts while the foundation is considered as rigid behaviour (Fig.A5). As present in Section 4.1.3, seven (7) licit mechanisms are considered (Fig.A6). However, only the study on the mechanisms "e" and "f" (Fig.A6) are presented herein, the calculation of the other mechanisms can be found in the literature, e.g [1], [3].

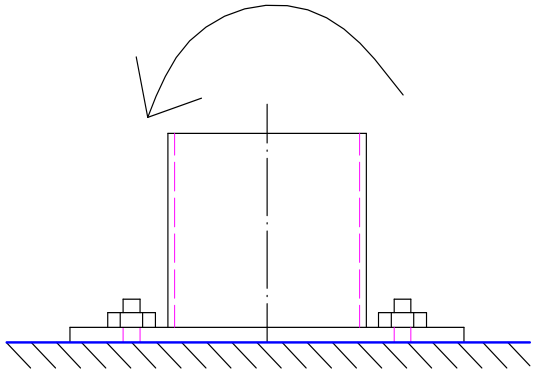

Fig.A5. Column base in limit analysis

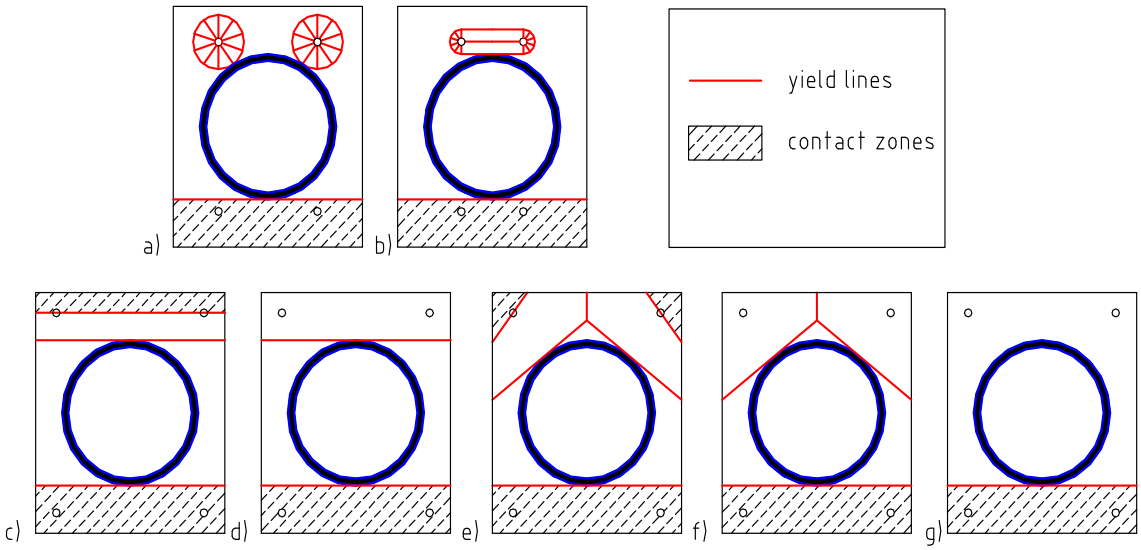

Fig.A6: Column base - considered mechanisms for the end plate

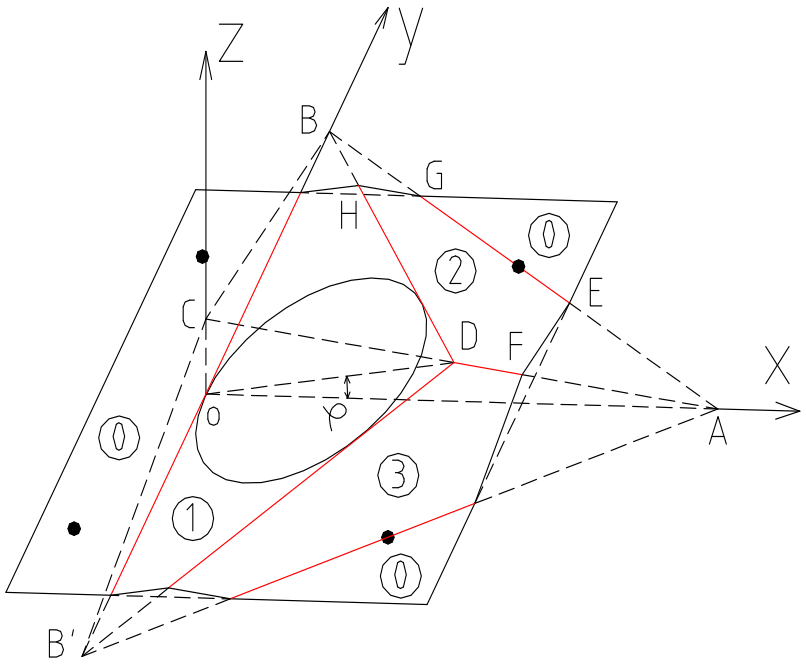

Fig.A7. Mechanism “e” family

Fig.A7 details the geometries of the mechanism “e”. In fact, this is a family of mechanism where the difference of its members is the position of point B on the y axe (or position of the point A on x axe). Six (6) yield lines are formed and the end plate is devised into four (4) rigid planes: plane o (ABB’), plane 1 (DBB’), plane 2 (ABD), and plane 3 (AB’D). It needs to find the optimal mechanism (real mechanism) in this family, on the other word, it should find the optimal position of point B (or A). The virtual work principle is applied and the main formulas are presented in Tables A.1, A.2 and A.3 below.

Table A.1: Main equations for limit analysis of the investigated structure

Equation	**Eq. number**	**Indication**
$W_E = W_I$	(A7)	Virtual work principle
$W_E = M\varphi$	(A8)	External work
$W_I = m_p \sum \theta_{ij} l_{ij}$	(A9)	Internal work
$m_p = t_p^2 f_y / 4$	(A10)	Unit plastic moment of the end plate
$l_{ij} = \sqrt{l_{ij,x}^2 + l_{ij,y}^2}$	(A11)	Length of the yield line ij between plane i and plane j; with $l_{ij,x}$, $l_{ij,y}$ are the components of l_{ij} on the x and y axis, respectively.
$\theta_{ij} \approx \dfrac{\mathbf{n}_i \times \mathbf{n}_j}{\mathbf{n}_i \bullet \mathbf{n}_j}$	(A12)	Rotation of the yield line ij between plane i and plane j; with $\mathbf{n}_i$ and $\mathbf{n}_j$ are the normal vectors of the plane i and plane j respectively.

Table A.2: determination of n_i, n_j, $l_{ij,x}$ and $l_{ij,y}$

plane i – plane j	$\mathbf{n}_i$	$\mathbf{n}_j$	$l_{ij,x}$	$l_{ij,y}$
0-1	$0\mathbf{i}+0\mathbf{j}+1\mathbf{k}$	$-z_D\mathbf{i}+0\mathbf{j}+x_D\mathbf{k}$	0	$y_G-y_{G'}$
0-2	$0\mathbf{i}+0\mathbf{j}+1\mathbf{k}$	$x_A^{-1}\mathbf{i}+y_B^{-1}\mathbf{j}+z_C^{-1}\mathbf{k}$	x_E-x_G	y_G-y_E
0-3	$0\mathbf{i}+0\mathbf{j}+1\mathbf{k}$	$x_A^{-1}\mathbf{i}+y_{B'}^{-1}\mathbf{j}+z_C^{-1}\mathbf{k}$	x_E-x_G	y_G-y_E
1-2	$-z_D\mathbf{i}+0\mathbf{j}+x_D\mathbf{k}$	$x_A^{-1}\mathbf{i}+y_B^{-1}\mathbf{j}+z_C^{-1}\mathbf{k}$	x_D-x_H	y_H-y_D
2-3	$x_A^{-1}\mathbf{i}+y_B^{-1}\mathbf{j}+z_C^{-1}\mathbf{k}$	$x_A^{-1}\mathbf{i}+y_{B'}^{-1}\mathbf{j}+z_C^{-1}\mathbf{k}$	x_F-x_D	0

All above geometric quantities (in Table A.2) can be written under the functions of y_B, as the present in Table A3.

Table A3: the coordinates of the point A, B, C, D, E, F, G, H following y_B.

Quantities	**Equation**
x_D	$x_D=0.5d'\{1+\cos[2artg(d'/(2y_B)\}/\cos\{2artg[d'/(2y_B)]\}$
x_A	$x_A=y_B[(y+d'/2)/(y_B-e/2)]$
z_D	$z_D=\varphi x_D$
$y_{B'}$	$y_{B'}=y_B$
z_c	$z_C=x_Ax_D/(x_A-x_D)$
y_G	$y_G=b/2$
$y_{G'}$	$y_{G'}=-b/2$
X_E	$x_E=d'+n'+e_1$
x_G	$x_G=x_A[1-b/(2y_B)]$
y_E	$y_E=y_B[x_A-(d'+n'+e_1)]/x_A$
x_H	$x_H=x_D(y_B-b/2)/y_B$
y_H	$y_H=b/2$
x_F	$x_F=x_E$

Now, the virtual work principle of Eq.(A7) can be written as: $M = W_I(y_B)$.

And the optimal mechanism is found by solving the following, Eq.A13:

$$\frac{dW_i}{dy_B} = 0 \rightarrow \text{optimal mechanism}. \tag{A13}$$

In principle, the analytical solution of Eq.(A13) can be obtain, however its explicit form is quite complicated. Therefore, for the reason of practical application, in this work, Eq.(A13) is solved by the numerical way. The moment (M_{p5} in Table 3) is written as $M_{p5} = \alpha_1 b m_p$ and the coefficient α_1 can be numerically determined. The geometric dimensions of the end plate, the tube and the bolt position are varied such that almost practical cases may be covered: $b/d' = 1,2 \div 2,0$; $h/b = 1,0 \div 1,6$; $\beta = m'/(\sqrt{e_1^2 + e_2^2} + m') = 0,3 \div 0,7$ (β concerns the bolt position). The bolts are supposed be on the diagonal of the end plate. α_1 is given in Table A4.

The same analysis (from the basis equations to the numerical calculations) are carried out for the mechanism "f " and the coefficients α_2 and α_3 (see Table A3) are given in Tables A5 and A6, respectively.

Noting that in mechanisms "e" and "f" the prying force is taken into account. If the prying force is not considered, the mechanism "f" is modified and the coefficient α_4 (see Table A7) can be obtained and given in Table A7.

Table A4: coefficient α_1

β	h/b	b/d'								
		1,2	1,3	1,4	1,5	1,6	1,7	1,8	1,9	2,0
0,3	1,0	19,373	17,194	15,561	14,277	13,234	12,373	11,640	11,005	10,467
	1,1	18,447	16,512	15,019	13,833	12,861	12,050	11,259	10,494	9,849
	1,2	17,694	15,939	14,561	13,375	12,181	11,214	10,415	9,740	9,167
	1,3	17,078	15,311	13,618	12,306	11,259	10,406	9,695	9,094	8,581
	1,4	15,981	14,029	12,556	11,402	10,475	9,714	9,077	8,538	8,075
	1,5	14,654	12,953	11,653	10,628	9,800	9,116	8,543	8,055	7,634
	1,6	13,537	12,036	10,880	9,962	9,216	8,598	8,076	7,631	7,247
0,4	1,0	14,222	12,660	11,492	10,576	9,836	9,226	8,708	8,264	7,881
	1,1	13,543	12,151	11,089	10,247	9,560	8,990	8,500	8,080	7,717
	1,2	12,974	11,721	10,745	9,962	9,319	8,780	8,316	7,849	7,418
	1,3	12,505	11,352	10,449	9,714	8,988	8,347	7,813	7,362	6,976
	1,4	12,110	11,040	9,959	9,093	8,397	7,825	7,347	6,942	6,594
	1,5	11,535	10,256	9,280	8,511	7,888	7,375	6,944	6,576	6,260
	1,6	10,694	9,567	8,699	8,009	7,448	6,983	6,591	6,257	5,967
0,5	1,0	11,139	9,943	9,052	8,357	7,798	7,339	6,950	6,619	6,332
	1,1	10,601	9,537	8,732	8,096	7,581	7,151	6,786	6,475	6,201
	1,2	10,144	9,192	8,457	7,869	7,387	6,982	6,638	6,344	6,083
	1,3	9,766	8,894	8,215	7,668	7,214	6,832	6,506	6,224	5,975
	1,4	9,441	8,640	8,006	7,491	7,062	6,698	6,314	5,989	5,709
	1,5	9,166	8,420	7,823	7,246	6,747	6,334	5,988	5,693	5,439
	1,6	8,930	8,091	7,395	6,842	6,392	6,018	5,704	5,435	5,203
0,6	1,0	9,087	8,133	7,426	6,878	6,439	6,081	5,778	5,522	5,299
	1,1	8,639	7,796	7,161	6,663	6,261	5,925	5,643	5,402	5,192
	1,2	8,259	7,507	6,931	6,472	6,097	5,785	5,521	5,291	5,094
	1,3	7,939	7,258	6,728	6,302	5,952	5,659	5,408	5,191	5,002
	1,4	7,666	7,041	6,551	6,153	5,824	5,545	5,306	5,100	4,919
	1,5	7,432	6,853	6,394	6,020	5,708	5,443	5,215	5,018	4,843
	1,6	7,229	6,689	6,257	5,902	5,604	5,351	5,113	4,888	4,694
0,7	1,0	7,620	6,837	6,264	5,821	5,469	5,182	4,940	4,738	4,561
	1,1	7,238	6,552	6,039	5,639	5,316	5,050	4,827	4,635	4,470
	1,2	6,913	6,304	5,840	5,474	5,177	4,929	4,720	4,540	4,384
	1,3	6,635	6,088	5,665	5,327	5,050	4,819	4,622	4,452	4,305
	1,4	6,397	5,900	5,510	5,197	4,938	4,720	4,533	4,373	4,232
	1,5	6,193	5,735	5,373	5,080	4,836	4,630	4,453	4,300	4,165
	1,6	6,016	5,591	5,252	4,976	4,745	4,549	4,380	4,233	4,105

Table A5: coefficient α_2

β	h/b	b/d'								
		1,2	1,3	1,4	1,5	1,6	1,7	1,8	1,9	2
	1,0	4,981	4,508	4,170	3,916	3,718	3,559	3,428	3,318	3,225
	1,1	4,716	4,312	4,017	3,792	3,614	3,470	3,350	3,250	3,164
	1,2	4,482	4,132	3,872	3,671	3,511	3,381	3,272	3,179	3,100
	1,3	4,276	3,969	3,739	3,558	3,413	3,294	3,194	3,109	3,036
	1,4	4,093	3,822	3,616	3,453	3,321	3,212	3,120	3,042	2,974
	1,5	3,932	3,690	3,504	3,356	3,235	3,135	3,050	2,977	2,914
	1,6	3,788	3,571	3,402	3,266	3,156	3,063	2,984	2,916	2,857

Table A6: coefficient α_3

β	h/b	b/d'								
		1,2	1,3	1,4	1,5	1,6	1,7	1,8	1,9	2,0
0,3	1,0	0,515	0,480	0,447	0,418	0,392	0,371	0,350	0,334	0,317
	1,1	0,528	0,489	0,455	0,426	0,402	0,378	0,359	0,340	0,324
	1,2	0,535	0,498	0,464	0,434	0,409	0,385	0,365	0,347	0,330
	1,3	0,545	0,505	0,472	0,441	0,415	0,391	0,371	0,352	0,336
	1,4	0,552	0,511	0,477	0,447	0,421	0,397	0,376	0,357	0,340
	1,5	0,559	0,518	0,483	0,453	0,425	0,402	0,380	0,362	0,344
	1,6	0,565	0,523	0,488	0,457	0,430	0,406	0,385	0,365	0,348
0,4	1,0	0,441	0,412	0,383	0,358	0,336	0,318	0,300	0,286	0,271
	1,1	0,453	0,419	0,390	0,365	0,344	0,324	0,308	0,291	0,278
	1,2	0,459	0,427	0,397	0,372	0,350	0,330	0,313	0,298	0,283
	1,3	0,467	0,433	0,404	0,378	0,356	0,335	0,318	0,302	0,288
	1,4	0,474	0,438	0,409	0,383	0,361	0,341	0,322	0,306	0,292
	1,5	0,479	0,444	0,414	0,388	0,365	0,345	0,326	0,310	0,295
	1,6	0,484	0,448	0,418	0,392	0,369	0,348	0,330	0,313	0,298
0,5	1,0	0,368	0,343	0,319	0,298	0,280	0,265	0,250	0,238	0,226
	1,1	0,377	0,349	0,325	0,304	0,287	0,270	0,256	0,243	0,232
	1,2	0,382	0,356	0,331	0,310	0,292	0,275	0,261	0,248	0,236
	1,3	0,389	0,361	0,337	0,315	0,297	0,279	0,265	0,252	0,240
	1,4	0,395	0,365	0,341	0,319	0,301	0,284	0,269	0,255	0,243
	1,5	0,399	0,370	0,345	0,323	0,304	0,287	0,272	0,258	0,246
	1,6	0,403	0,374	0,349	0,327	0,307	0,290	0,275	0,261	0,248
0,6	1,0	0,294	0,274	0,255	0,239	0,224	0,212	0,200	0,191	0,181
	1,1	0,302	0,279	0,260	0,243	0,229	0,216	0,205	0,194	0,185
	1,2	0,306	0,285	0,265	0,248	0,234	0,220	0,209	0,198	0,188
	1,3	0,312	0,289	0,269	0,252	0,237	0,223	0,212	0,201	0,192
	1,4	0,316	0,292	0,273	0,256	0,240	0,227	0,215	0,204	0,194
	1,5	0,319	0,296	0,276	0,259	0,243	0,230	0,217	0,207	0,197
	1,6	0,323	0,299	0,279	0,261	0,246	0,232	0,220	0,209	0,199
0,7	1,0	0,221	0,206	0,192	0,179	0,168	0,159	0,150	0,143	0,136
	1,1	0,226	0,210	0,195	0,182	0,172	0,162	0,154	0,146	0,139
	1,2	0,229	0,213	0,199	0,186	0,175	0,165	0,156	0,149	0,141
	1,3	0,234	0,216	0,202	0,189	0,178	0,168	0,159	0,151	0,144
	1,4	0,237	0,219	0,205	0,192	0,180	0,170	0,161	0,153	0,146
	1,5	0,240	0,222	0,207	0,194	0,182	0,172	0,163	0,155	0,148
	1,6	0,242	0,224	0,209	0,196	0,184	0,174	0,165	0,157	0,149

Table A7: coefficient α_4

β	h/b	b/d'								
		1,2	1,3	1,4	1,5	1,6	1,7	1,8	1,9	2
0,3	1,0	12,601	10,931	9,729	8,820	8,110	7,531	7,057	6,662	6,321
	1,1	11,539	10,116	9,072	8,273	7,640	7,100	6,640	6,256	5,930
	1,2	10,625	9,400	8,475	7,715	7,114	6,625	6,221	5,882	5,593
	1,3	9,836	8,694	7,842	7,181	6,653	6,222	5,864	5,561	5,303
	1,4	9,036	8,053	7,310	6,728	6,261	5,877	5,556	5,284	5,051
	1,5	8,371	7,513	6,858	6,342	5,924	5,579	5,290	5,044	4,832
	1,6	7,810	7,054	6,471	6,008	5,632	5,320	5,057	4,833	4,639
0,4	1,0	9,856	8,616	7,724	7,051	6,524	6,097	5,746	5,454	5,203
	1,1	9,085	8,027	7,252	6,658	6,188	5,806	5,491	5,224	4,997
	1,2	8,417	7,504	6,825	6,299	5,879	5,519	5,215	4,960	4,742
	1,3	7,840	7,045	6,431	5,934	5,537	5,213	4,943	4,715	4,520
	1,4	7,327	6,588	6,029	5,592	5,240	4,951	4,709	4,504	4,328
	1,5	6,825	6,180	5,688	5,299	4,984	4,724	4,506	4,320	4,160
	1,6	6,402	5,833	5,394	5,046	4,762	4,527	4,329	4,159	4,013
0,5	1,0	8,219	7,236	6,530	5,996	5,579	5,243	4,966	4,735	4,537
	1,1	7,619	6,780	6,165	5,695	5,323	5,021	4,772	4,561	4,381
	1,2	7,097	6,373	5,834	5,417	5,085	4,813	4,586	4,395	4,230
	1,3	6,645	6,013	5,537	5,165	4,866	4,614	4,397	4,213	4,056
	1,4	6,252	5,695	5,267	4,916	4,633	4,400	4,206	4,041	3,899
	1,5	5,904	5,386	4,990	4,678	4,425	4,216	4,040	3,890	3,761
	1,6	5,562	5,105	4,752	4,472	4,244	4,055	3,895	3,758	3,640
0,6	1,0	7,134	6,322	5,739	5,298	4,954	4,678	4,450	4,259	4,097
	1,1	6,646	5,952	5,444	5,057	4,750	4,501	4,295	4,121	3,973
	1,2	6,221	5,622	5,177	4,832	4,557	4,333	4,146	3,987	3,852
	1,3	5,852	5,329	4,935	4,627	4,379	4,176	4,005	3,860	3,735
	1,4	5,529	5,068	4,717	4,440	4,216	4,030	3,872	3,733	3,613
	1,5	5,246	4,836	4,521	4,266	4,053	3,878	3,730	3,604	3,495
	1,6	4,998	4,622	4,326	4,091	3,900	3,740	3,606	3,491	3,391
0,7	1,0	6,361	5,670	5,175	4,803	4,511	4,276	4,083	3,921	3,784
	1,1	5,954	5,363	4,932	4,603	4,342	4,131	3,956	3,809	3,683
	1,2	5,598	5,088	4,709	4,416	4,182	3,991	3,832	3,698	3,582
	1,3	5,287	4,842	4,506	4,244	4,033	3,860	3,715	3,591	3,485
	1,4	5,015	4,622	4,323	4,086	3,895	3,737	3,604	3,491	3,393
	1,5	4,776	4,426	4,157	3,943	3,769	3,624	3,501	3,397	3,304
	1,6	4,564	4,251	4,007	3,812	3,653	3,515	3,399	3,299	3,213

A5.2. Validation

The results of the above development are compared with the experimental tests within WP3 (See Deliverable D3). Three specimens with the variation of the end plate thickness were tested with the main parameters of the specimens are presented in Table A8. The calculations using the present development of moments M_y and M_u (by using f_y and f_u respectively) are summarized in Table A9. The mechanism "e" occurs according to both analytical and experimental investigations. The Figs.A8-A10 shows that the present results are in agreement with the experimental ones.

Table A8: Geometries and material of the specimens (the symbols can be found on Fig.A1)

Specimen	Geometries (mm)								Material strength (N/mm2)	
	b	h	t_p	d	e_1	e_2	w	a	f_y	f_u
1	400	400	14	193.7	60	60	23.685	16	418	602
2	400	400	16	193.7	60	60	23.685	16	418	602
3	400	400	18	193.7	60	60	23.685	16	418	602

Table A9: calculation of M_y and M_u

Specimen	b/d'	h/b	β	B mm	m_y Nmm/mm	m_u Nmm/mm	α_1 (Table A4)	M_y (kNm)	M_u (kNm)
1	1.74	1	0.5	400	20482	29498	7,18	59	85
2	1.74	1	0.5	400	26752	38528	7,18	77	111
3	1.74	1	0.5	400	33858	48762	7,18	97	140

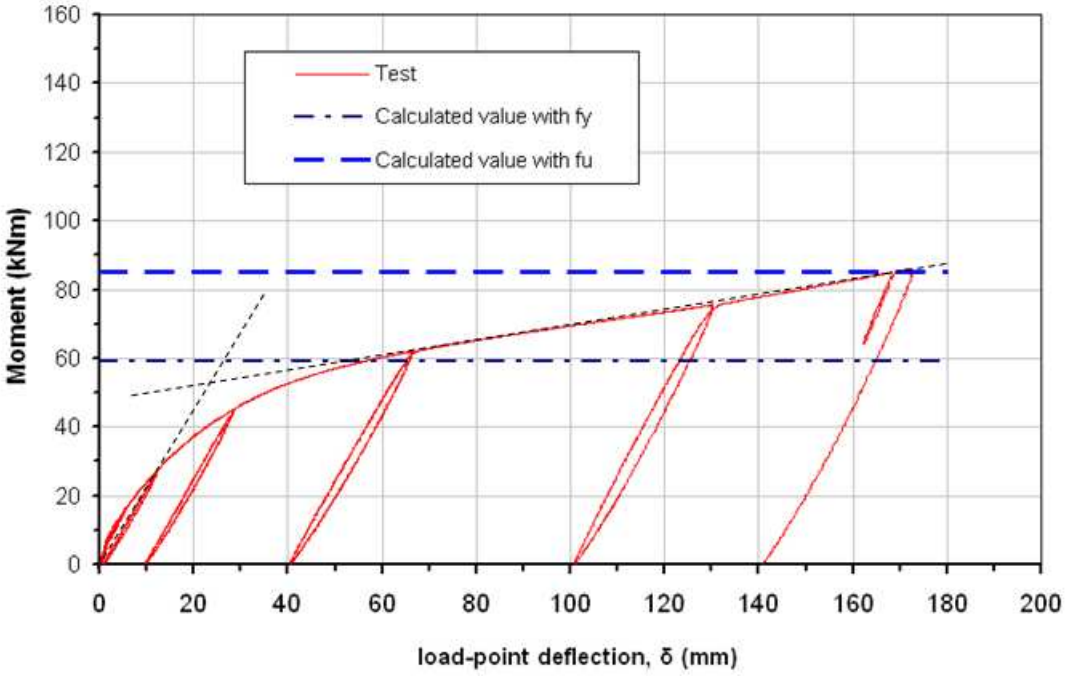

Fig.A8. Comparison for specimen 1

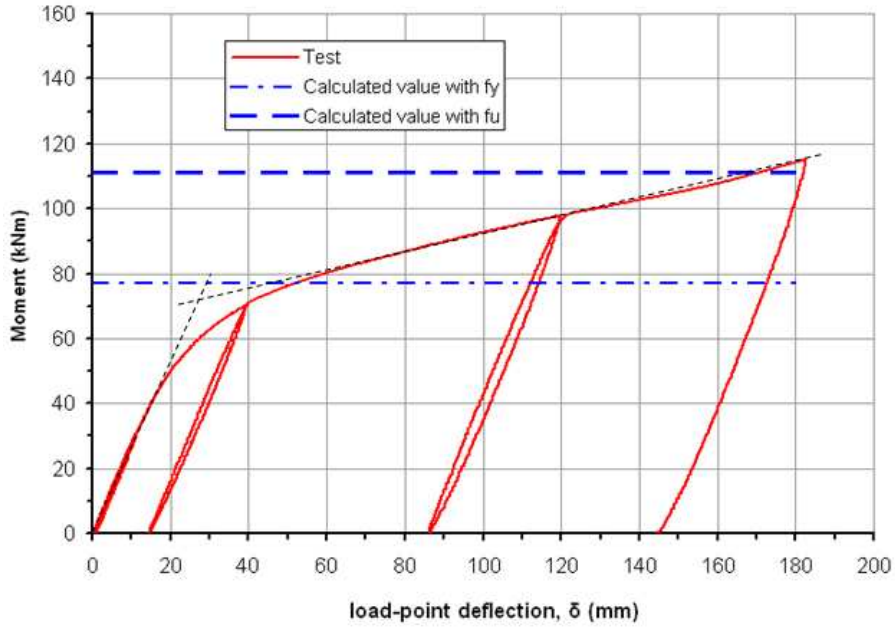

Fig.A9. Comparison for specimen 2

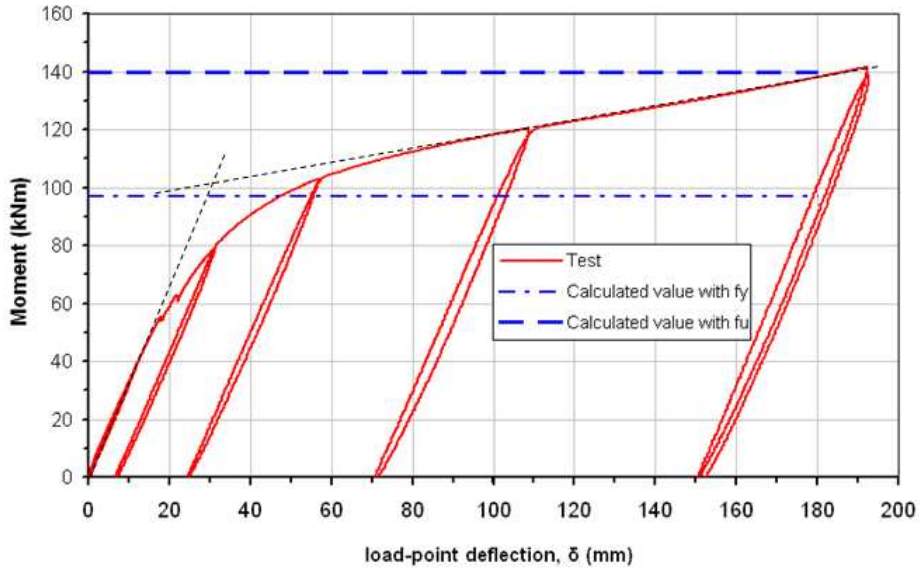

Fig.A10. Comparison for specimen 3

A.6. Conclusion

The resistance determination of the column base by using the component methods is presented. In particular, based on the limit analysis, the practical calculation for the "plate in bending, bolts in tension" component of the column base is proposed. The results are in agreement with the experimental one.

References for Appendix A

[1] Eurocode 3: Design of steel structures - Part 1-8: Design of joints. EN 1993-1-8, Brussels, 2003.

[2] Guisse S, Vandegans D, Jaspart JP. Application of the component method to column bases – experimentation and development of a mechanical model for characterization. Research Centre of the Belgian Metalworking Industry, 1996.

[3] Jaspart JP. Recent advances in the field od steel joints column bases and further configurations for beam-to-column joints and beam splices. Agregation Thesis, University of Liege, 1997.

Appendix B: **Through plate of static joint**

B1. Introduction

This appendix details Section 5.1.3, on the development for the through plate of the static joint.

B2. Notices (Fig.B1)

t: thickness of the plate;

h: height of the plate;

b: width of the plate part outside the tube;

D: inside diameter of the tube;

F_{Ed}: design value of the horizontal component of the load;

V_{Ed}: design value of the vertical component of the load;

α: load direction;

E: Young modulus;

υ: Poisson ratio.

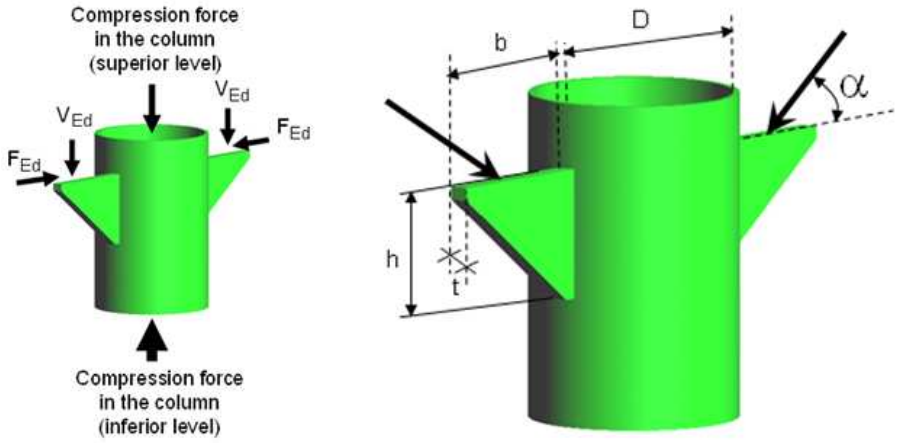

Fig.B1. Beam-to-column joints - through plate component

B3. General considerations and hypotheses

Fig.B2 describes the buckling mode of the whole joint while the buckling mode of the through plate is shown on the Fig.B3.

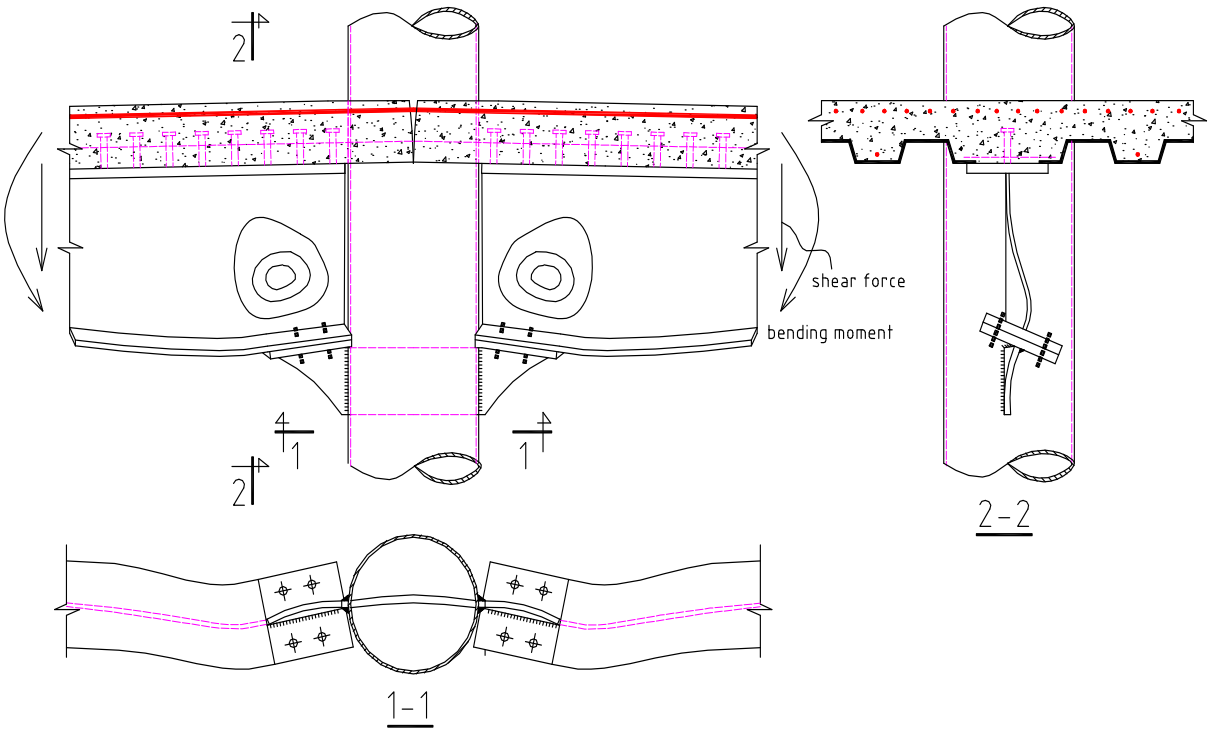

Fig.B2. Buckling mode of joint

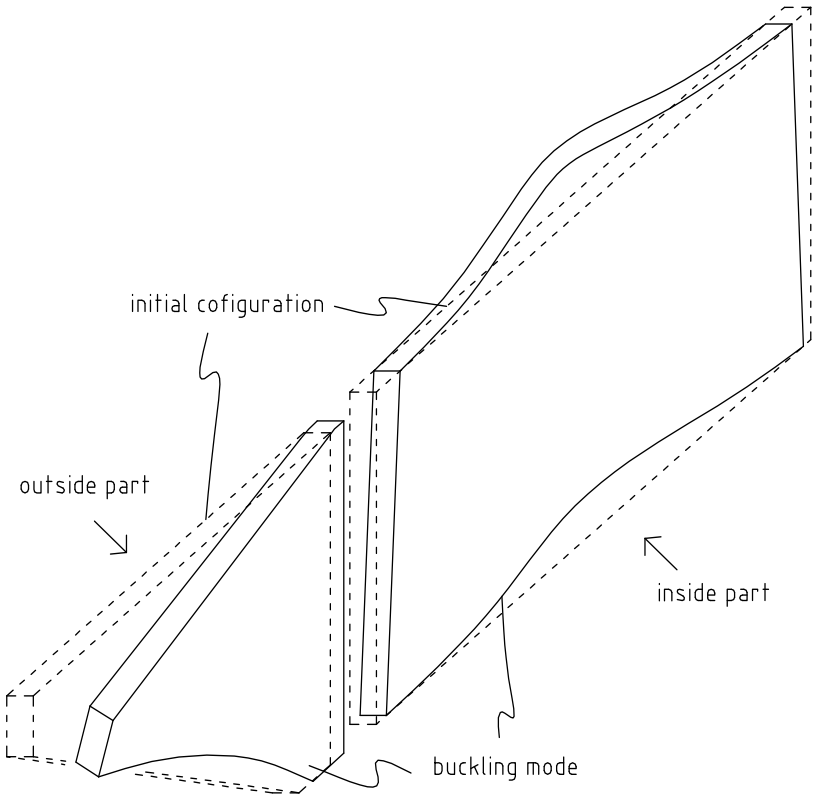

Fig.B3. Buckling mode of through plate

For the simplification reason, the through plate is devised into two parts, inside part (inside the column) and outside parts (outside the column) with the boundary and loading condition as the show on Fig.B3. The buckling theory of plate is applied to study the strength of each part.

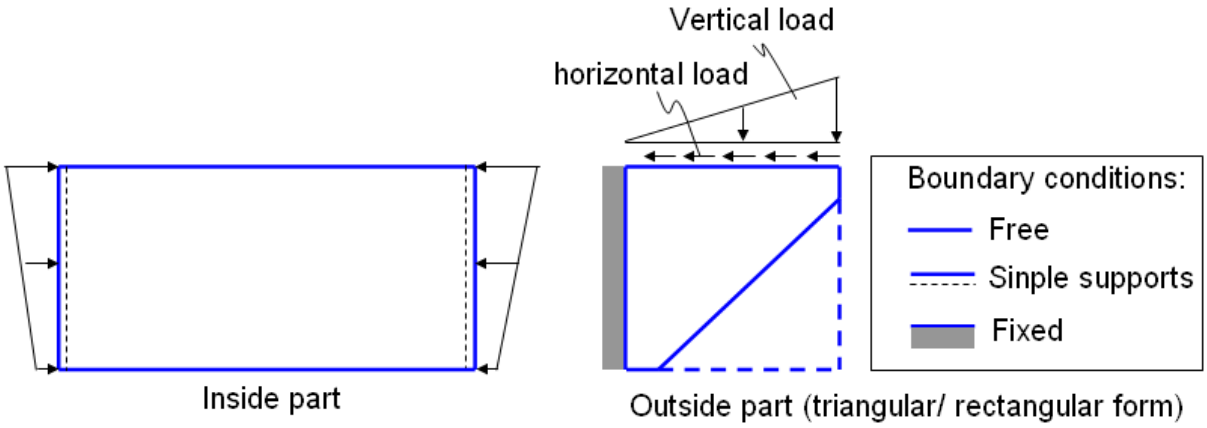

Fig.B4. modelling of boundary and loading for the through plate

B4. Design of the through plate

Using the buckling theory of plates, the buckling stresses of the inside and outside parts can be written by Eqs.(B1) and (B2) as follows:

$$\sigma_{c,ou} = \mu_1 \frac{\pi^2 E}{12(1-\nu^2)}\left(\frac{t}{b}\right)^2; \tag{B1}$$

$$\sigma_{c,in} = \mu_2 \frac{\pi^2 E}{12(1-\nu^2)}\left(\frac{t}{h}\right)^2. \tag{B2}$$

The coefficients μ_1 and μ_1 in Eqs. (B1) and (B2) are used to take into account boundary condition, loading condition, plasticity and initial imperfection. In this work, these coefficients are determined by the numerical analysis, as Eqs.(B3) and (B4):

$$\mu_1 = (\sigma_{c,ou})_{numerical} \Big/ \left(\frac{\pi^2 E}{12(1-\nu^2)}\left(\frac{t}{b}\right)^2\right); \tag{B3}$$

$$\mu_2 = (\sigma_{c,in})_{numerical} \Big/ \left(\frac{\pi^2 E}{12(1-\nu^2)}\left(\frac{t}{h}\right)^2\right), \tag{B4}$$

with $\sigma_{numerical}$ is calculated by LAGAMINE (a nonlinear finite element code developed in University of Liege) considering the boundary condition, the loading, the plasticity and the initial imperfection, as the description on Figs.B5 and B6. The detail on the numerical strategy and its validation are presented in WP5 (see Deliverable D5). The parametric study (the geometric dimensions of the plate are varied such that almost practical case can be coved) is performed, and the corresponding values of μ_1 and μ_1 are obtained.

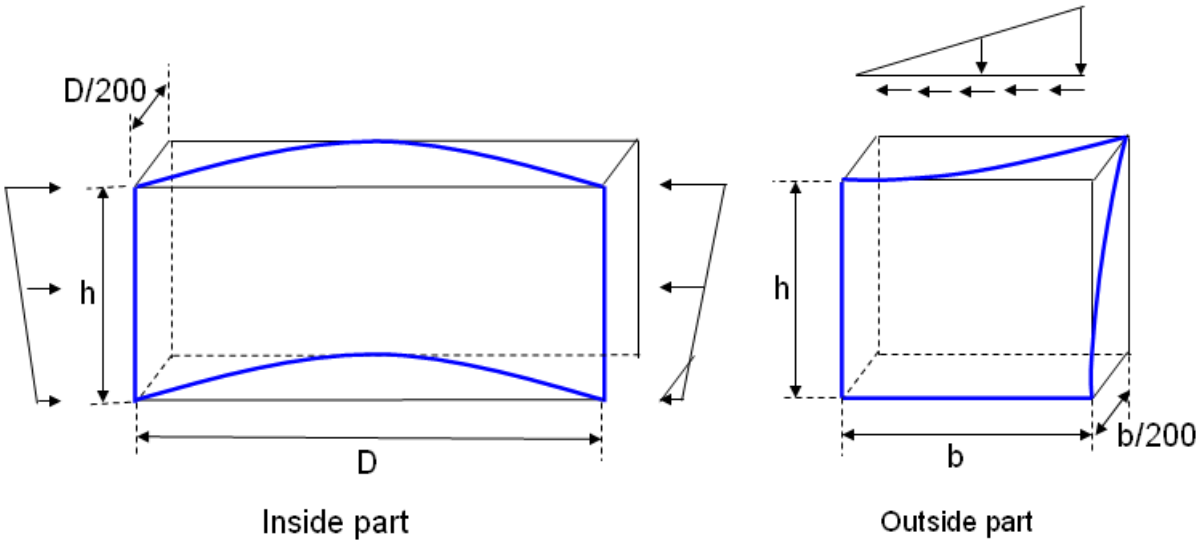

Fig.B5. modeling of the initial imperfection for the plate

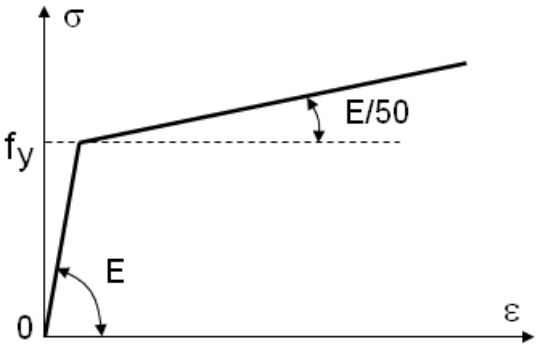

Fig.B6. Material modelling in the numerical analysis

Finally, the safety verification of the through plate may be performed by the following formula:

$$\begin{cases} \dfrac{V_{Ed}}{th} \le \kappa\mu_1 \dfrac{\pi^2 E}{12(1-\upsilon^2)}\left(\dfrac{t}{b}\right)^2 / \gamma_{M1}; \\ \dfrac{4F_{Ed}}{th} + \dfrac{4V_{Ed}b}{th^2} \le \mu_2 \dfrac{\pi^2 E}{12(1-\upsilon^2)}\left(\dfrac{t}{h}\right)^2 / \gamma_{M1}. \end{cases} \quad \text{(B5)}$$

with γ_{M1} is the partial factor according to EN1993-1-1 [1]; κ= 1.0 for the rectangular outside part and κ = 0.9 for the triangular outside part; μ_1 and μ_2 are given in Tables B1 and B2. Three loading types in Table B2 is shown on Fig.B7, in which σ_{max} and σ_{min} are calculated as follows (Eq.(B6)):

$$\sigma_{\max} = \frac{4V_{Ed}b}{th^2} - \frac{4F_{Ed}}{th}; \quad \sigma_{\min} = \frac{4V_{Ed}b}{th^2} + \frac{4F_{Ed}}{th} \quad \text{(B6)}$$

.

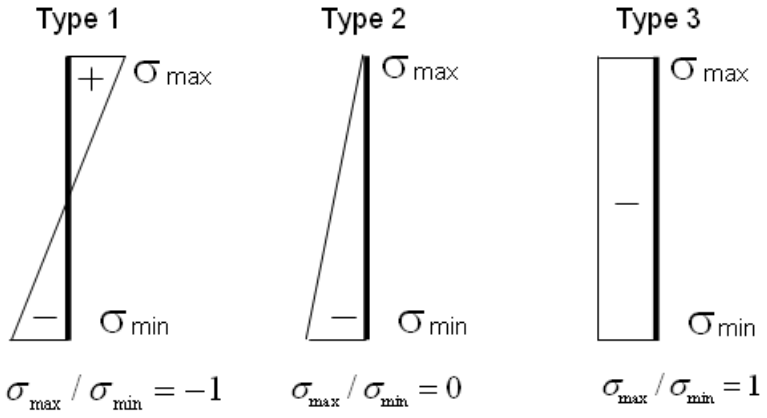

Fig.B7: loading type for the inside part of the plate

Noting that the value of μ_1 and μ_2 given in Tables 1 and 2 are only validated for S355 steel.

Table B1: Buckling stress factor for outside plate (μ_1)

Geometries		Load direction α (in degree)				
h/b	t/b	α=90	α=60	α=45	α=30	α=15
0,6	0,505	0,1686	0,1591	0,1718	0,1654	0,0632
	0,075	0,1027	0,0887	0,0871	0,0840	0,0397
	0,100	0,0763	0,0610	0,0589	0,0531	0,0302
	0,125	0,0661	0,0475	0,0433	0,0381	0,0213
	0,150	0,0546	0,0402	0,0343	0,0304	0,0185
0,8	0,050	0,2455	0,2518	0,2487	0,1654	0,0717
	0,075	0,1467	0,1343	0,1308	0,1080	0,0465
	0,100	0,1027	0,0902	0,0844	0,0677	0,0337
	0,125	0,0801	0,0672	0,0620	0,0488	0,0255
	0,150	0,0699	0,0543	0,0492	0,0384	0,0225
1,0	0,050	0,3151	0,3246	0,2750	0,1675	0,0790
	0,075	0,1820	0,1758	0,1636	0,1115	0,0525
	0,100	0,1263	0,1117	0,0985	0,0778	0,0370
	0,125	0,0908	0,0812	0,0742	0,0591	0,0293
	0,150	0,0744	0,0640	0,0582	0,0464	0,0260
1,2	0,050	0,3762	0,3857	0,2792	0,1739	0,0843
	0,075	0,2042	0,2039	0,1964	0,1230	0,0568
	0,100	0,1317	0,1263	0,1142	0,0829	0,0419
	0,125	0,0961	0,0893	0,0807	0,0637	0,0331
	0,150	0,0715	0,0691	0,0624	0,0520	0,0288
1,4	0,050	0,4194	0,4278	0,2792	0,1770	0,0875
	0,075	0,2217	0,2535	0,1789	0,1190	0,2869
	0,100	0,1386	0,1374	0,1191	0,0844	0,0436
	0,125	0,0993	0,0943	0,0859	0,0658	0,0348
	0,150	0,0786	0,0713	0,0654	0,0546	0,0304

Table B2: Buckling stress factor for inside plate (μ_2)

Geometries		Load type (Fig.B7)		
D/b	t/h	type 1	type 2	type 3
1,00	0,050	1,0875	0,7819	0,4805
	0,075	0,5620	0,4409	0,2779
	0,100	0,2792	0,2761	0,1710
	0,125	0,1794	0,1794	0,1145
	0,150	0,1246	0,1246	0,0826
1,15	0,050	1,0474	0,6997	0,4173
	0,075	0,5364	0,4146	0,2785
	0,100	0,2792	0,2632	0,1644
	0,125	0,1794	0,1794	0,1111
	0,150	0,1246	0,1246	0,0795
1,33	0,050	1,0495	0,6006	0,4152
	0,075	0,5208	0,3828	0,3072
	0,100	0,2792	0,2487	0,1617
	0,125	0,1794	0,1731	0,1146
	0,150	0,1246	0,1246	0,0846
1,67	0,050	1,0116	0,4636	0,2466
	0,075	0,5358	0,3335	0,1886
	0,100	0,2792	0,2358	0,1370
	0,125	0,1794	0,1794	0,1196
	0,150	0,1246	0,1208	0,0731
2,00	0,050	0,9800	0,3498	0,1834
	0,075	0,5189	0,2760	0,1636
	0,100	0,2792	0,2044	0,1175
	0,125	0,1794	0,1511	0,0924
	0,150	0,1246	0,1133	0,0729

B5. Conclusions

The formulas for design of the through plate of the static joints are proposed. These formulas are based on the elastic plate buckling formulation while the plasticity, the boundary conditions, the loading ways and the initial imperfection are taken into account by numerical analysis. The parametric study is also carried out on the geometric dimensions of the plate.

References for Appendix B

[1] Eurocode 3: Design of steel structures, Part 1-1: General rules and rules for buildings. EN 1993-1-1, Brussels, 2005.

Appendix C: Cross-Sectional Strength of high-strength steel tubular members

EN 1993-1-1 provisions classify high-strength steel CHS members with relatively low values of D/t ratio as Class 3 or 4, so that their strength is based on elastic behavior only, neglecting their capability of sustaining inelastic deformation before a maximum resistance is reached. To investigate the applicability of the above classification, a special-purpose numerical technique is employed to examine the resistance against local buckling of high-strength steel seamless tubular members with significant thickness, that exhibit local buckling in the plastic regime under axial compression and bending. The numerical technique employs large inelastic strains, accounts for the presence of initial imperfections/residual stresses, and is capable of describing deformation and buckling of tubular cross-sections well beyond yielding of the steel material. Imperfections and residual stresses from real measurements are used. Numerical results are presented in terms of both the ultimate load and the deformation capacity of typical cross-sections, and are compared with available experimental data. The results aim at evaluating the applicability of EN 1993-1-1 for cross-sectional classification of high-strength steel CHS seamless tubular members.

C1-Introduction

High-strength steel CHS tubes are becoming popular in a variety of structural engineering applications, such as tubular columns of building systems or members of tubular lattice structures. The principal characteristic of these steel products, with respect to CHS tubes of normal steel grades, is the elevated yield stress value, which implies increased ultimate capacity, resulting in a good relationship between weight and strength. They can also be efficient in cases where space occupancy becomes a critical design criterion.

According to current design practice, the ultimate capacity of steel sections under axial and bending loads depends primarily on whether the section is classified as “compact” or “non-compact”, i.e. on the ability of the cross-section to sustain significant inelastic deformation before failure in the form of local buckling. In particular, the provisions of EN 1993-1-1 standard specify four (4) cross-sectional classes, where Class 4 corresponds to thin-walled sections, which are able to sustain axial/bending load only in the elastic range, Class 1 includes thick-walled sections that are able to deform well into the plastic regime, without exhibiting local buckling, and Classes 2 and 3 refer to intermediate type of structural behavior. For the case of CHS tubular members, classification in EN 1993-1-1 is based on the value of the diameter-to-thickness ratio, as well as on the value of the material yield stress, as shown in the second column of Table 1. The same classification is also adopted by the CIDECT guidelines [16] for hollow section stability, whereas similar provisions for cross-sectional classification on CHS members can be found in other specifications (e.g. AISC, API RP2A – LRFD).

The above classification provisions do not cover the case of high-strength steel CHS tubular members. In the EN 1993 steel design framework, a new standard has been issued EN 1993-1-12 to specify the applicability of the other EN 1993-1-xx standards in high-strength steel applications. According to EN 1993-1-12, the EN 1993-1-1 classification provisions may be applied for high-strength steel members as well. However, the existing classification for CHS tubular members appears to be quite penalizing for high-strength steel tubular members; one can readily obtain from Table 1 that CHS sections with D/t = 35 and σ_Y =690 MPa, are classified as Class 4 sections, which implies a low ultimate capacity, within the elastic range.

The key issue in the above classification of CHS members is their cross-sectional strength, mainly in terms of local buckling, which constitutes a shell-buckling problem in the inelastic range. Inelastic buckling of relatively thick-walled steel cylinders under compressive loads has been the issue of significant research. Experimental observations ([4] and [13]) have been shown that under pure axial compression, thick-walled cylinders – in contrast with thin-walled ones – do not fail abruptly, but one can observed significant wall wrinkling before an ultimate load occurs. Analytically, a main challenge for solving this problem has been the combination of structural stability principles with inelastic multi-axial material behavior. In particular, it has been shown that buckling predictions depend on the choice of plasticity theory [17]. For a detailed presentation of metal cylinder buckling behavior under uniform axial compression, the reader is referred to the recent papers ([2] & [3]).

In addition to uniform axial compression, bending buckling of tubular members has also received significant attention, motivated mainly by their use in pipeline applications. Experimental works indicated that failure of thick-walled tubes under bending is associated with tube wall wrinkling, has

several similarities with the case of uniform axial compression, but is characterized by a nonlinear prebuckling state – due to cross-sectional ovalization – and a more localized buckling pattern on the compression side of the cylinder. The reader is also referred to the papers [10] and [11], where analytical/numerical tools have been developed for simulating the formation of local buckling due to bending.

The present research aims at a examining the cross-sectional classification of high-strength steel CHS seamless tubular members, and is part of an extensive European research on the structural behavior of high-strength steel tubular members. The same high-strength steel tubes have also been considered in [15] in terms of their structural beam-column behavior, and the need for a more accurate classification of high-strength steel CHS sections has been addressed.

The investigation described in the present paper is numerical, based on a special-purpose finite element formulation, presented elsewhere [11], and focuses on the buckling analysis of high-strength steel cylindrical shells under axial compression and bending loading. The analysis steps are aimed at determining the maximum load at which failure occurs, either because of bifurcation to a wavy pattern or due to localization of deformation.

The seamless tubes under consideration have yield stress equal or higher than 590 MPa, and diameter-to-thickness ratios ranging between 20 and 60, which are typical for structural applications. Initial imperfections and residual stresses from real measurements are taken into account in the present analysis. The numerical results are presented in the form of diagrams, showing the cylinder strength and deformation capacity (axial and bending) in terms of cylinder slenderness, and are aimed towards a evaluating applicability of existing classification rules for high-strength steel CHS tubes.

Table C1. Classification in EN 1993-1-1, based on the value of the diameter-to-thickness ratio

Class	Class limits	Class limits in terms of shell slenderness λ
1	$D/t \le 50\varepsilon^2$	$\lambda \le \lambda_1 = 0.278$
2	$50\varepsilon^2 \le D/t \le 70\varepsilon^2$	$\lambda_1 = 0.278 < \lambda \le \lambda_2 = 0.329$
3	$70\varepsilon^2 \le D/t \le 90\varepsilon^2$	$\lambda_2 = 0.329 < \lambda \le \lambda_3 = 0.373$
4	$D/t \ge 90\varepsilon^2$	$\lambda > \lambda_3 = 0.373$

C2-Numerical technique

C2.1Formulation and finite element discretization

The nonlinear formulation adopted in the present work was introduced in its general form by Needleman (1982) [14] and has been employed for the nonlinear analysis of relatively thick steel tubular members [11]. The cylindrical shell is considered as a continuum, described through a Lagrangian approach with convected coordinates. The hypoelastic constitutive equations relate the convected rate of Kirchhoff stress to the rate-of-deformation tensor, where plasticity effects are taken into account through a large-strain J_2 flow plasticity model with isotropic hardening. Following classical shell theory, the traction component normal to any shell lamina is imposed to be zero and tube thickness is assumed constant.

Discretization of the continuum is considered through the use of the three-node "tube element", introduced in [11]. It couples longitudinal (beam-type) with cross-sectional deformation (ovalization and warping). Convected coordinates (θ, ζ, ρ) are in the hoop, axial and radial direction in the undeformed configuration. Nodes are located along the cylinder axis, which lies on the plane of bending, and each node possesses three degrees of freedom (two translational and one rotational). A reference line is chosen within the cross-section at node (k) and a local Cartesian coordinate system is defined, so that the $\bar{x}, \bar{y}$ axes define the cross-sectional plane. The orientation of node (k) is defined by the position of three orthonormal vectors $\mathbf{e}_x^{(k)}, \mathbf{e}_y^{(k)}$ and $\mathbf{e}_z^{(k)}$. For in-plane (ovalization) deformation, fibers initially normal to the reference line remain normal to the reference line. Furthermore, those fibers may rotate in the out-of-plane direction by angle $\gamma(\theta)$. Using quadratic interpolation

polynomials $N^{(k)}(\zeta)$ in the longitudinal direction, the position vector $\mathbf{x}(\theta,\zeta,\rho)$ of an arbitrary point at the deformed configuration is:

$$\mathbf{x}=\sum_{k=1}^{3}\left[\left(\mathbf{x}^{(k)}+\mathbf{r}^{(k)}(\theta)+\rho\mathbf{n}^{(k)}(\theta)+\rho\gamma(\theta)\mathbf{e}_z^{(k)}\right)N^{(k)}(\zeta)\right] \tag{C1}$$

where $\mathbf{x}^{(k)}$ is the position vector of node (k), $\mathbf{r}^{(k)}(\theta)$ is the position of the reference line of cross-section corresponding to node (k),and $\mathbf{n}^{(k)}(\theta)$ is the "in-plane" outward normal of the reference line at the deformed configuration. Using nonlinear ring theory, $\mathbf{r}^{(k)}(\theta)$ and $\mathbf{n}^{(k)}(\theta)$ can be expressed in terms of the radial, tangential and out-of-plane displacements of the reference line, denoted as $w(\theta)$, $v(\theta)$ and $u(\theta)$ respectively. Functions $w(\theta)$, $v(\theta)$, $u(\theta)$ and $\gamma(\theta)$ are discretized as follows:

$$w(\theta)=a_0+a_1\sin\theta+\sum_{n=2,4,\ldots}a_n\cos n\theta+\sum_{n=3,5,..}a_n\sin n\theta \tag{C2}$$

$$v(\theta)=-a_1\cos\theta+\sum_{n=2,4,6,\ldots}b_n\sin n\theta+\sum_{n=3,5,7,\ldots.}b_n\cos n\theta \tag{C3}$$

$$u(\theta)=\sum_{n=2,4,6,\ldots}c_n\cos n\theta+\sum_{n=3,5,7,\ldots.}c_n\sin n\theta \tag{C4}$$

$$\gamma(\theta)=\sum_{n=0,2,4,6,\ldots}\gamma_n\cos n\theta+\sum_{n=1,3,5,7,\ldots.}\gamma_n\sin n\theta \tag{C5}$$

Coefficients a_n, b_n refer to in-plane cross-sectional (ovalization) deformation, whereas c_n, γ_n refer to out-of-plane (warping) cross-sectional deformation.

The nonlinear governing equations are solved through an incremental Newton-Raphson iterative numerical procedure, enhanced to enable the tracing of postbuckling "snap-back" equilibrium paths through an arc-length algorithm [9].

C.2.2.Bifurcation in the inelastic range

Bifurcation instability in axially or bending loaded shells in the inelastic range is checked o, through the evaluation of Hill's "comparison solid" functional, as described in [9]. Loss of positive definiteness of this functional determines the buckling load. Positive definiteness is evaluated through an eigenvalue analysis on the pre-buckling solution, and the corresponding eigenfunction is the buckling shape (mode) of the cylinder.

C.2.3 Material moduli for buckling calculations

Early attempts to predict the buckling load of relatively-thick metal shells ([4] and [13]) indicated that analytical predictions are in closer agreement with test results when J_2 deformation-plasticity theory moduli are employed, instead of the classical J_2 flow-plasticity moduli. This has been verified in more recent works [2], and is attributed to the "softer" moduli of the deformation theory, simulating a "vertex" or "corner" (i.e. a high-curvature region on the yield surface at the point of loading), reported in experimental observations, whereas flow theory assumes always a smooth yield surface, resulting in "stiffer" material moduli for case of abrupt change of direction in the stress space (e.g. when buckling occurs). To account for this discrepancy, the J_2-flow theory is used to trace the load-displacement equilibrium path, as described in section C.2.1, whereas the J_2-deformation moduli are employed to detect bifurcation in the eigenvalue analysis of the "comparison solid" functional, as described in section C.2.2.

C.2.4 Initial imperfections and residual stresses

The finite element model is capable of including the effects of initial imperfections, by prescribing a desired configuration of the shell in the initial (reference) stage. In the present analysis, the initial imperfection is assumed in a wavy form, similar to the buckling shape obtained from the bifurcation analysis on the pre-buckling equilibrium path. In addition to initial imperfections, the finite element model accounts for the presence of residual stresses, which have a significant effect on the buckling load. The amplitudes of initial imperfections and residual stresses are obtained from the corresponding measurements described in the next section.

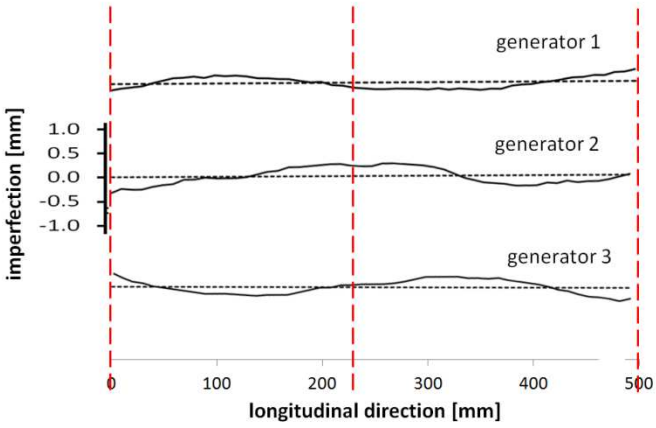

(a)

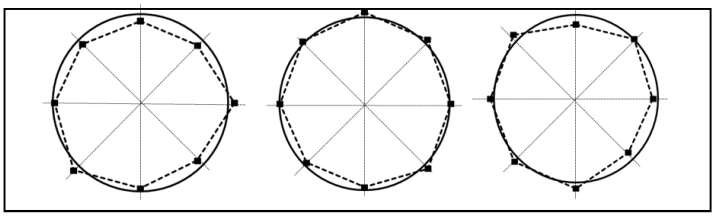

(b)

Figure C1. Typical data from (a) measurement of generator geometry (b) out-of-roundness of three cross-sections.

C.3 Imperfection measurements

C.3.1 Imperfection measurements

Initial wrinkling measurements have been obtained using an ultrasonic device. The tube wall wrinkling was measured every 10 mm along 8 equally-spaced generators, for a pipe length of 500 mm, as shown in Figure C1(a), for three typical generators.

These measurements along generators have been processed to estimate initial wrinkling as well as cross-sectional distortions; i.e. out-of-roundness imperfections when a specific cross section is considered.

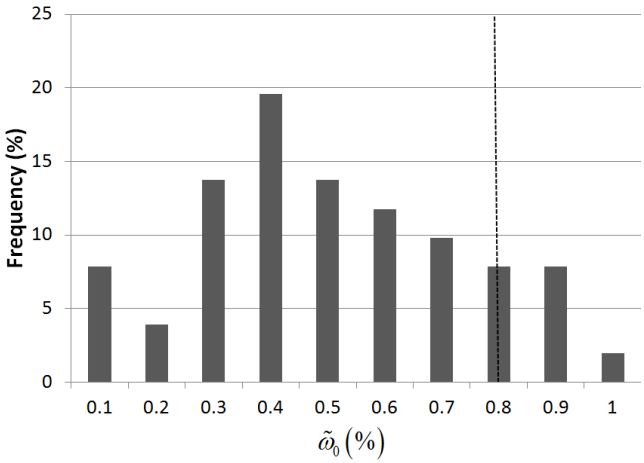

Figure C2. Statistical evaluation of $\tilde{\omega}_0$, the measured absolute-value amplitude of the axisymmetric imperfection.

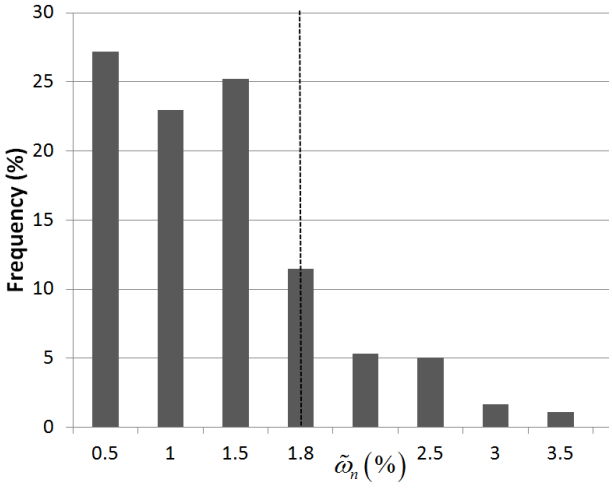

Figure C3. Statistical evaluation of $\tilde{\omega}_n$, the measured absolute-value amplitude of the non-axisymmetric imperfection.

It is assumed that the deviation of every cross-section from the perfect round shape is the superposition of an "extensional" component of uniform value around the cross-section, which can axisymmetric initial imperfection, and non-uniform part which corresponds to cross-sectional out-of-roundness in Figure C1(b). In Figures C2 and C3, $\tilde{\omega}_0$ and $\tilde{\omega}_n$ represent the measured amplitudes of the axisymmetric and the non-uniform imperfection components respectively with respect to tube thickness. A statistical evaluation of $\tilde{\omega}_0$ and $\tilde{\omega}_n$ is offered in those Figures; the values of $\tilde{\omega}_0 = 0.8\%$ and $\tilde{\omega}_n = 1.8\%$ correspond to an 80% upper limit of the measurements, and are considered as representative initial imperfection values to be used the parametric study described in the next section.

C.3.2 Residual Stresses

Residual stress measurements have also been performed in both the axial and the circumferential direction [15]. The measurements in the hoop direction are obtained through the "splitting ring" method, as specified in ASTM E1928-99, and resulted in an opening deformation (gap) of 1.7 mm, corresponding to a maximum hoop stress of 122 MPa (about 16% of the yield stress). Furthermore, to estimate the residual stresses in the axial direction, longitudinal strips have been obtained from the tubes, and their curvature has been measured, corresponding to a maximum stress of 26 MPa, which is only 4% of the yield stress.

C.4 Numerical results

Results are obtained for 355.6-mm-diameter high-strength-steel tubes with thickness ranging between 6.4 mm and 16 mm covering a wide range of structural CHS sections. Two materials with yield stress equal to 590 MPa and 735 MPa are used, with nearly constant hardening modulus equal to $E/40$ [15].

C.4.1 Methodology for axial loading

Infinitely long cylindrical shells with axisymmetric and non-axisymmetric initial imperfections are analyzed. Non-axisymmetric modes and bifurcations along the equilibrium path are identified by the implementation of the ''tube-element''. Experimental observations as well as numerical results have shown that first wrinkling in the plastic range is axisymmetric. The corresponding bifurcation load and wavelength can be calculated analytically using equations C6 and C7.

$$\sigma_{cr} = \left[\frac{C_{11}C_{22} - C_{12}^2}{3}\right]^{1/2} \left(\frac{t}{R}\right) \tag{C6}$$

$$L_{hw} = \left[\frac{C_{11}^2}{12\left(C_{11}C_{22} - C_{12}^2\right)}\right]^{1/4} \left(Rt\right)^{1/2} \tag{C7}$$

where R and t are the radius and wall thickness of the tube and $C_{a\beta}$ are the instantaneous material moduli according to J_2 deformation plasticity theory, at the bifurcation stage [12].

The present analysis follows the steps described in [2]. Assuming a half-wave length from equation (C8), axisymmetric wrinkling on the prebuckling state for the uniformly-compressed cylinder is determined. Then, considering a tube segment of length equal to twice the value of half-wavelength ($L = 2L_{hw}$), and an axisymmetric initial imperfection, secondary bifurcation to a non-axisymmetric mode is calculated. In this analysis, the axisymmetric imperfection amplitude ω_0 is 0.8%, as indicated by the measurements (section C.3).

Subsequently, two possible limit states are examined. First, localization of the axisymmetric wrinkling pattern is examined, using a tube segment of length equal to several half-wavelengths. Considering a small bias in the amplitude of one wrinkle, the analysis leads to a maximum load N_1 due to wrinkle localization denoted as limit state (a). In addition, a tube segment of length equal to two half-wavelenghts with a combination of axisymmetric and non-axisymmetric imperfections is analyzed, with relative amplitudes ω_0 and ω_n equal to 0.8% and 1.8% respectively, so that a maximum load N_n is obtained. The smallest value of N_1 and N_n determines the ultimate axial load (strength) of the cross-section N_u .

C.4.2 Methodology for bending loading

The second part of this study concerns the prediction of ultimate capacity under bending loading, following the analysis steps described in [10]. The analysis is similar to the one in axial loading described above. At first, wrinkling on the ovalization bending prebuckling state is determined, and the corresponding half-wavelength is computed (L_{hw}). Then, using an initial imperfection on a tube segment of length equal to $2L_{hw}$, secondary bifurcation is calculated.

Subsequently, two possible limit states are examined, following a methodology similar to the one described for axial loading; (a) localization of wrinkling pattern and (b) analysis under a combination of imperfection corresponding to initial and secondary buckling modes. The minimum value from the corresponding maximum moments M_1 and M_n determines the ultimate moment of the cross-section, denoted as M_u .

C.4.3 Parametric study

The above advanced numerical tools are used to examine buckling of cylindrical high-strength steel shells under pure axial compressive load and pure bending. The cylindrical shells are thick-walled with properties shown in Table C2.

Table C2. Geometric and mechanical properties of tubes

Tube	t (mm)	D/t *	σ_y (MPa)	λ	Class**
1	6.4	55.56	735	0.517	4
2	8.0	44.45	735	0.463	4
3	10.0	35.56	735	0.414	4
4	12.5	28.45	735	0.370	3
5	14.2	25.05	735	0.347	3
6	16	22.22	735	0.327	2
7	14.2	25.05	590	0.311	2
8	16	22.22	590	0.293	2

** D is equal to 355.6 mm for all tubes*
*** According to EN-1993-1-1*

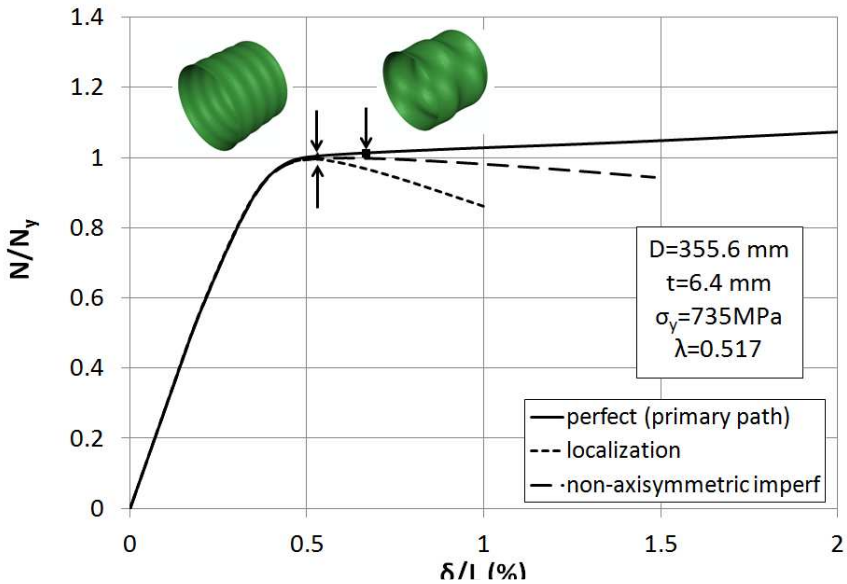

Figure C4. Axial load – displacement diagram of Tube 1.

The behavior is summarized schematically in the axial load-displacement response of the thin-walled Tube 1 in Figure C4, whereas the behavior of Tube 4 is shown in Figure C5. The load is normalized with the value $N_Y = \sigma_Y A$, where A and σ_Y are the cross sectional area and the yield stress, respectively. The reported displacement is normalized by the tube length. At some displacement level indicated by the first "↓" on the response, first axisymmetric wrinkling is calculated. Secondary bifurcation to a non-axisymmetric mode on the primary path is calculated indicated by the second "↓". The paths corresponding to the two possible limit states are examined, as described in section C.4.1. The ultimate axial load (strength) of the cross-section N_u, is equal to N_1, for the localization analysis and is indicated by the arrow "↑" in the two graphs.

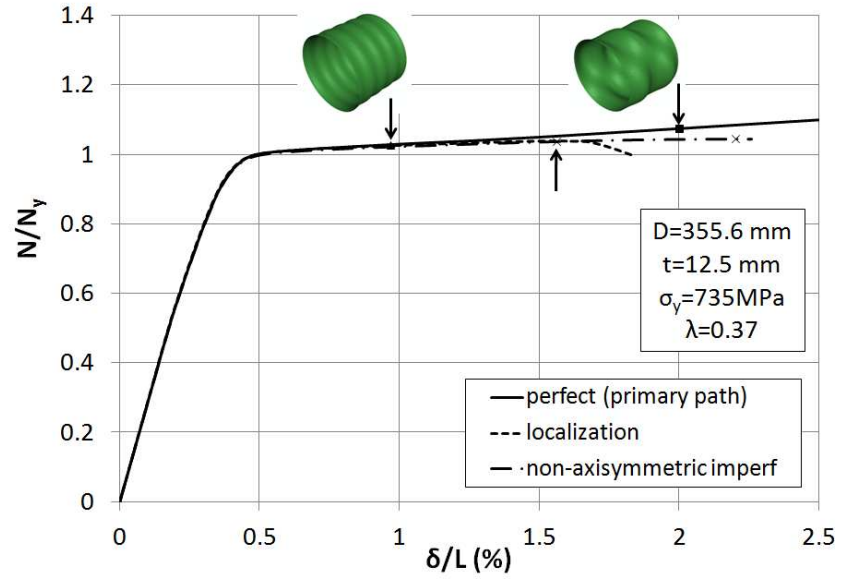

Figure C5. Axial load – displacement diagram of Tube 4.

The bending behavior is shown in the moment- curvature response of Tube 1 in Figure C6 and of Tube 4 in Figure C7. The moment is normalized by the fully-plastic moment ($M_p = \sigma_Y t D^2$) and the curvature is normalized by the value of characteristic value $k_i = t/D^2$.

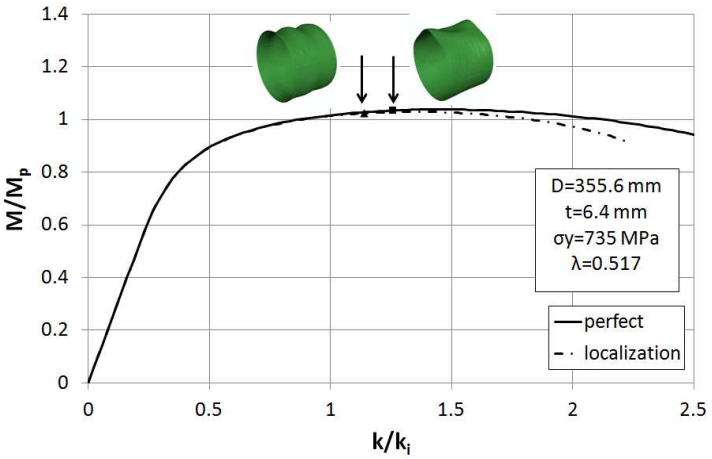

Figure C6. Moment-curvature diagram of thin-walled Tube 1.

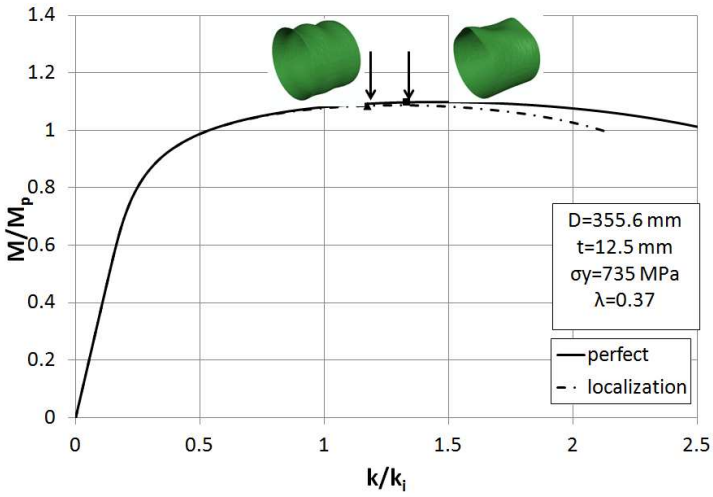

Figure C7. Moment-curvature diagram of Tube 4.

C.5 Experimental Results

Some limited experimental results on the high-strength steel CHS seamless tubes under consideration are also reported, for verification purposes. The tests have been conducted by CSM, and comprise three (3) tests with uniform axial compression, and two (2) tests on bending. The tubes have cross-sections denoted as A, B and C (see Table C3), and a steel material with yield stress equal to 735 MPa. The slenderness values for sections A, B and C are equal to 0.370, 0.395 and 0.305. The axial load tests failed because of buckle development in the form of bulging near the welds, a typical failure mode for this type of loading. All three tests showed that they are capable of sustaining an axial load higher than the full plastic thrust of the section ($N/N_Y = 1.033$, 1.082 and 1.102 for sections A, B and C respectively). The two bending experiments on sections A and B, because of test set-up limitations, did not reach the local buckling stage. Nevertheless, it has been possible to bend the two tubes at curvature levels corresponding to bending moments higher than the fully plastic moment ($M/M_Y = 1.402$ and 1.438 for sections A and B respectively).

Table C3. Experimental results on the high-strength steel tubes

Section	D (mm)	t (mm)	Yield stress (MPa)	Ultimate thrust (kN)	Ultimate moment (kNm)
A	355.6	12.5	735	10254	1168.6
B	323.9	10	735	7961	805.93
C	193.7	10	735	4414	

C.6 Classification of HSS CHS members

C.6.1 Current design practice

Table C1 shows the classification of CHS tubular members according the EN 1993-1-1. For consistency with the present analysis, the slenderness limits have been also given in terms of the so-called "shell slenderness", defined as:

$$\lambda = \sqrt{\sigma_Y / \sigma_e} \tag{C8}$$

where

$$\sigma_e = 0.605 E C_x t / R \tag{C9}$$

is the elastic buckling stress, and the value of C_x is taken equal to 0.6, representing an infinitely long cylinder, free of boundary condition effects.

For Class 1, 2 and 3 CHS sections ($\lambda \le 0.373$), the ultimate axial compressive capacity N_u is equal to the fully-plastic axial load $N_Y = \sigma_Y A$, where A is the cross-sectional area. If the value of λ exceeds 0.372, then the cross-section is classified as Class 4, implying that buckling occurs in the elastic range, and its ultimate axial compressive capacity is calculated from the EN 1993-1-6 rules for buckling of cylindrical shells, as follows:

$$N_u = \sigma_{x,Rk} A \tag{C10}$$

where the buckling strength $\sigma_{x,Rk}$ can be written:

$$\sigma_{x,Rk} = \chi(\lambda)\sigma_Y \tag{C11}$$

The reduction function χ depends on shell slenderness as follows:

$$\chi(\lambda) = \begin{cases} 1 & \lambda \le 0.2 \\ 1 - 0.6\left(\dfrac{\lambda - 0.2}{\lambda_P - 0.2}\right) & 0.2 < \lambda \le \lambda_P \\ \alpha / \lambda^2 & \lambda > \lambda_P \end{cases} \tag{C12}$$

where, assuming excellent manufacturing quality

$$\alpha = \frac{0.62}{1 + 1.91\left(\Delta w_\kappa / t\right)^{1.44}} \tag{C13}$$

$$\Delta w_\kappa / t = (1/40)\sqrt{R/t} \tag{C14}$$

$$\lambda_P = 1.581\sqrt{\alpha} \tag{C15}$$

For the case of bending loading, Class 1 and 2 cross-sections have an ultimate moment capacity M_u equal to the plastic bending moment $M_P = \sigma_Y W_{pl}$, where W_{pl} is the plastic bending modulus of the cross-section. For Class 3 sections, M_u is equal to the elastic bending moment $M_Y = \sigma_Y W_{el}$, where W_{el} is the elastic bending modulus. Finally, for Class 4 CHS sections, M_u is equal to $\sigma_{x,Rk} W_{el}$, where $\sigma_{x,Rk}$ is calculated from equations (C11) - (C15) above.

C.6.2 Comparison with numerical results and test data

The above predictions of ultimate capacity are plotted against the finite element results and the test data, in Figures C8(a) for the axial compression and C8(b) for bending, with respect to the slenderness parameter λ. The ultimate axial load and bending moment values are normalized by N_Y and M_Y respectively. The comparison between numerical results, test data and design provisions indicates that the EN 1993 standard provides a rather conservative ultimate capacity in terms of both axial and bending moment for the value of initial imperfections assumed in the present study.

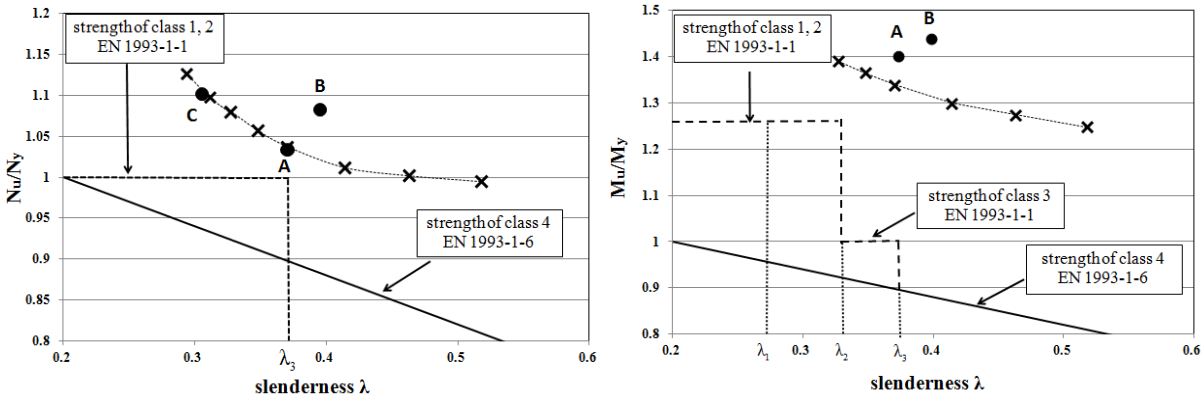

(a) (b)

Figure C8. Stability curves in comparison with EN1993-1-1 provision

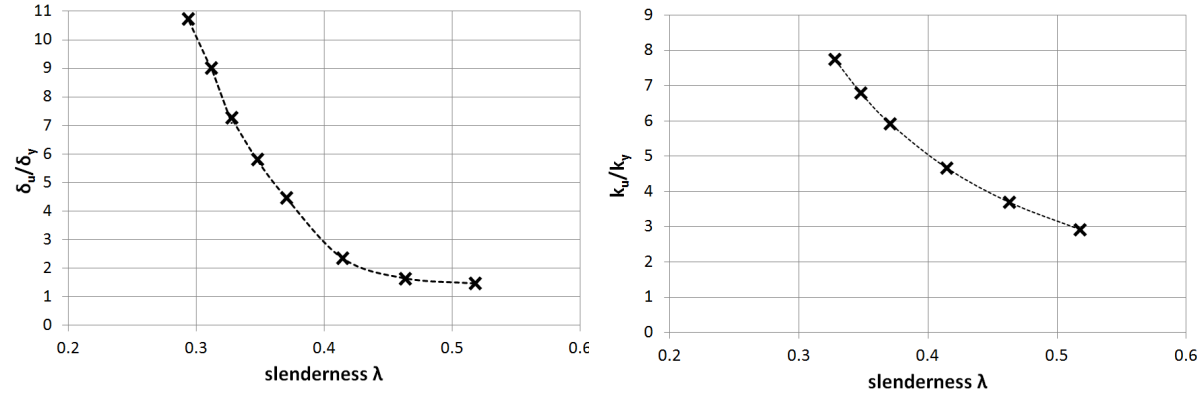

(a) (b)

Figure C 9. Deformation capacity of the cross-section for (a)axial and (b) moment load

In addition, Figures C9(a) and C9(b) show the numerical results for the deformation capacity of the cross-section for axial (δ_u) and bending (k_u) respectively, normalized by the corresponding values at yielding stage (δ_Y and k_Y), with respect to the value of λ. The values of δ_u and k_u correspond to N_u and M_u respectively. The values of δ_u/δ_Y and k_u/k_Y indicate significant deformation capacity of the tubes under consideration, well beyond first yielding.

C.7 Conclusions

Using a special-purpose numerical technique, wrinkling and post-wrinkling behavior of thick-walled high-strength CHS seamless tubular subjected to both bending and axial loading have been investigated, in order to determine their ability to sustain load above the first yield level. The results have been compared with limited test data, and with the EN 1993 classification provisions.

Considering imperfections and residual stresses obtained from real measurements on high-strength steel seamless tubes, the finite element results indicated significantly higher ultimate capacity with respect to the design rules of the above specification rules, as well as a substantial deformation capacity.

References for Appendix C

[1] American Institute of Steel Construction, 2005, "Steel Construction Manual" - Thirteenth Edition, AISC 325-05.

[2] Bardi, F.C., Kyriakides, S., 2006. "Plastic buckling of circular tubes under axial compression-part I: Experiments" *International Journal of Mechanical Sciences*, 48, 830-841.

[3] Bardi, F.C., Kyriakides, S., Yun, H.D., 2006. "Plastic buckling of circular tubes under axial compression-part II: Analysis" *International Journal of Mechanical Sciences*, 48, 842-854.

[4] Batterman, S. C., 1965. *Plastic buckling of axially compressed cylindrical shells*, AIAA Journal, 3, 316-325.

[5] EN 1993-1-1, 2005, "Eurocode 3: Design of steel structures. Part 1-1: General rules and rules for buildings." European Committee for Standardization.

[6] EN 1993-1-6, 2007, "Eurocode 3: Design of steel structures. Part 1-6: Strength and Stability of Shell Structures." European Committee for Standardization.
[7] EN 1993-1-12, 2007, "Eurocode 3: Design of steel structures. Part 1.12: Additional rules for the extension of EN 1993 up to steel grades S 700." European Committee for Standardization.
[8] Gellin, S., 1979. Effect of an axisymmetric imperfection on the plastic buckling of an axially compressed cylindrical shell, *ASME J. Appl. Mech*. 46, 125–131.
[9] Hutchinson, J.W., 1974. *Plastic buckling*, Advances n Applied Mechanics, 14, 67-144.
[10] Ju, G. T., Kyriakides, S., 1992. "Bifurcation and localization instabilities in cylindrical Shells under bending II: Predictions", *International Journal of Solids and Structures*, 29, 1143-1171.
[11] Karamanos, S.A., Tassoulas, J.L., 1996. "Tubular members I: stability analysis and preliminary results", *Journal of Engineering Mechanics*, ASCE, 122, 1, 64-71.
[12] Kyriakides, S., Corona, E., 2007, Mechanics of Offshore Pipelines, Vol. I Buckling and Collapse, Elsevier.
[13] Lee, L. N. H., 1962. *Inelastic buckling of initially imperfect cylindrical shells subjected to axial compression*, Journal of Aerospace Science 29 87–95.
[14] Needleman, A., 1982. "Finite elements for finite strain plasticity problems", *Plasticity of Metals at Finite Strain: Theory, Experiment and Computation*, edited by E.H. Lee and R.L. Mallet, Rensselaer Polytechnic Institute, Troy, New York, 387-436.
[15] Pournara, A. E.., Karamanos, S. A., Ferino, J., Lucci, A., 2012. Strength and stability of high-strength steel tubular beam-columns under compressive loading. *14th International Symposium On Tubular Structures*, Paper No. 104, London, UK.
[16] Rondal, J., Würker K.G., Dutta D. Wardenier J., Yeomans N., 1996, "Structural stability of hollow sections", CIDECT (Ed.) and Verlad TÜV Rheinland.
[17] Tvergaard, V., 1983. Plastic buckling of axially compressed circular cylindrical shells, *Int. J. Thin−Walled Struct*. 1, 139–163

Appendix D: FE Simulation-Interaction curves

D1. Buckling resistance of HSS CHS columns in bending and axial compression

Members under axial compression plus bending develop specific load-carrying behaviour in the different ranges of slenderness. Depending on the emphasis given to the different ranges, different concepts of interaction formulae have been proposed in the past. The present approach of EN1993-1-1 [1] is based on the linear-additive form of interaction formula derived from linear-elastic buckling response, where the effect of the axial force and the bending moments are linearly summed and the nonlinear effects are accounted for by specific interaction factors. Latest version of the Eurocode 3 has incorporated some new design formulae that enable a more economic design. This is particularly the case for the rules for the verification of members subjected to combined bending and compression.
Moreover Part 1-12 of Eurocode 3 [2] has been recently published that extends its scope to strength grades up to S700. Part 1-12 gives a few changes and some additional rules to the already existing parts of Eurocode 3 in order to make them applicable to steel grades up to S700.
Eurocode 3 design philosophy is based on cross sectional classification: depending on the compactness of the cross section and on its strength grade the ability of a member to experience full plastic resistance is assessed. The Eurocode 3 cross sectional classification was originally assessed on normal steel grades (S235, S355) and the recently developed Part 1-12 extend those formulation without extensive experimental validation. This results in a penalisation of HSS in terms of ductility: considering a certain CHS having D/t ratio of about 25-30 it is supposed to be able to develop plastic deformation without the occurrence of instability only if normal steel grade is concerned (Fig. D1).

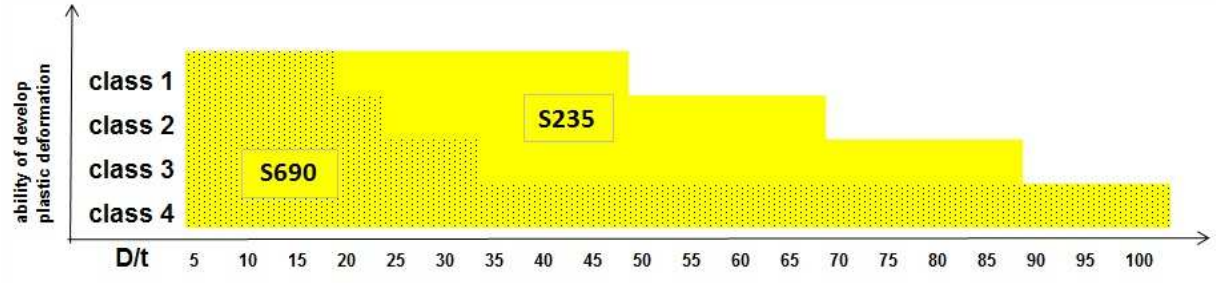

Figure D1: Eurocode 3 cross sectional classification: comparison between S235 and S690.

In the frame of this project two (2) different HSS CHS are studied, they are classified in Class 3 and Class 4 (Table D1) in accordance with Eurocode 3 while if normal steel grade was employed the same cross sections would be classified as Class 1.

Table D1. CHS studied in the project.

ID	diameter D [mm]	thickness t [mm]	D/t	Actual S690 Class	S235 Class
A	355	12	29.6	3	1
B	323.9	10	32.4	4	1

It is particularly penalising in the case of cross section B: being classified as Class 4 means that local instability is likely to occur before first yielding of the cross section, in this case the design falls into the EN1993-1-6 [2] where reduction coefficients shall be applied to design yield stress in fact reducing eventual benefices coming from HSS.

Full-scale tests have been performed on CHS members reported in Table D2 fabricated at two different lengths

- Short (member slenderness 15 and 17 for A and B respectively) relevant for cross sectional behaviour
- Long (member slenderness 40 and 44 for A and B respectively) relevant for member behaviour

The outcome of experimental data (task 3.3) extended with parametric studies (task 5.1) are compared with Eurocode 3 predictions in the following N-M interaction diagrams. The EC3 predictions are calculated following both methods presently reported in the standard, namely Method 1 (m1) and Method 2 (m2) [3], for the scope of comparison safety coefficients were set to 1.00 and actual yield stress was used. In Fig. D2 and Fig. D3 experimental results show to be always in the safe side of the interaction diagrams. In particular short member behaviour (Fig. D2) relevant for local instability and cross sectional classification shows the larger margin, especially in the case of cross section B due to the strength reduction factor (about 0.89 in the present case) imposed by the standard as previously explained. A comparison with design curves with and without the application of strength reduction factor (Class 4 and Class 3 respectivelly) is reported in Fig. D4

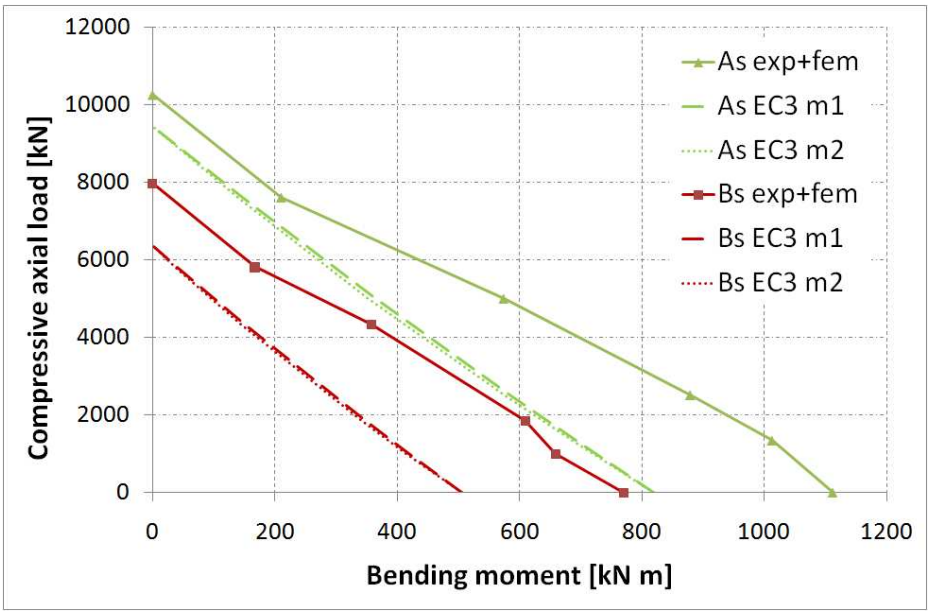

Figure D2: Short member interaction diagram: comparison with Eurocode 3 design recommendations.

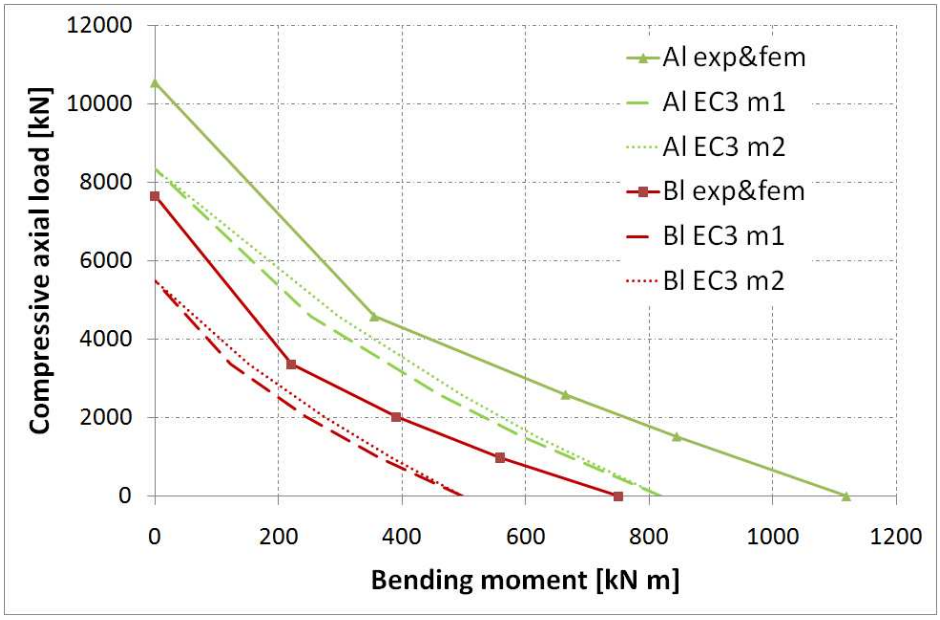

Figure D3: Long member interaction diagram: comparison with Eurocode 3 design recommendations.

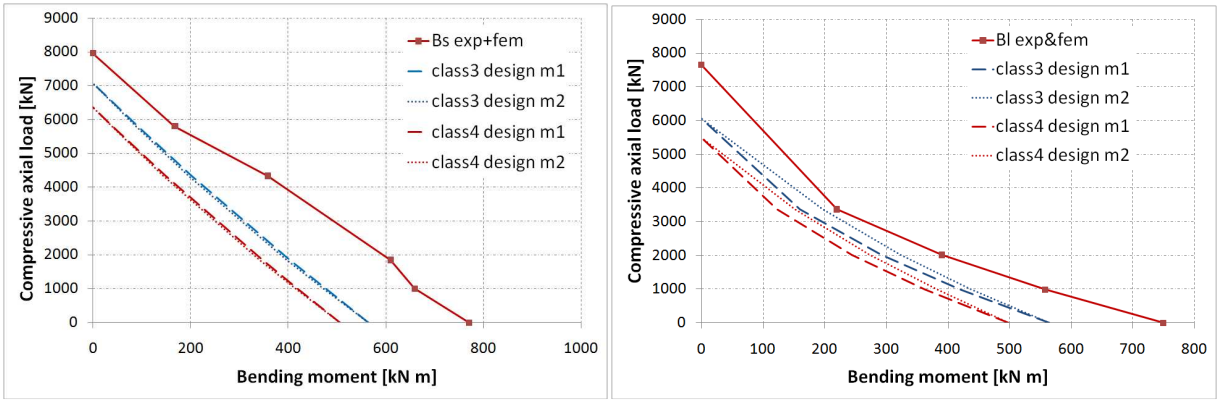

Figure D4: Cross section B specimens: comparison among experimental data and class 3 and class 4 design curves

Experimental data and finite element analysis outcomes are in this section presented in a form to make it consistent with Eurocode 3 interaction formulae. In particular second order moment imposed by extensions of the testing machine are explicitly reported as follow.
Full scale testing rig is such that the column is connected to the machine hinges via rigid extensions named “codolo” able to transmit rigid motion to the column ends (Fig. D5). In the case of combined load test where constant axial compressive load is applied, once the specimen starts to rotate a second order moment induced by “codolos” is applied at the column ends.

Figure D5: Full scale testing arrangement.

Experiment outcome report applied loads at the machine hinges hence moments induced by "codolos" are not explicitly quantified. This is an inconvenience when comparing experimental data with design interaction formulae that refers to the column loaded at its ends, as in the case of Eurocode 3.
Stating that "codolos" are much stiffer than column, knowing the rotation at the hinges, it is possible to explicitly show the second order moment induced by "codolos". The experimental curves modified with explicit contribution of "codolos" are reported In Fig. D6b -Fig. D9b for short and long members respectively, those were used for comparison with Eurocode 3 interaction formulae (Fig. D4).

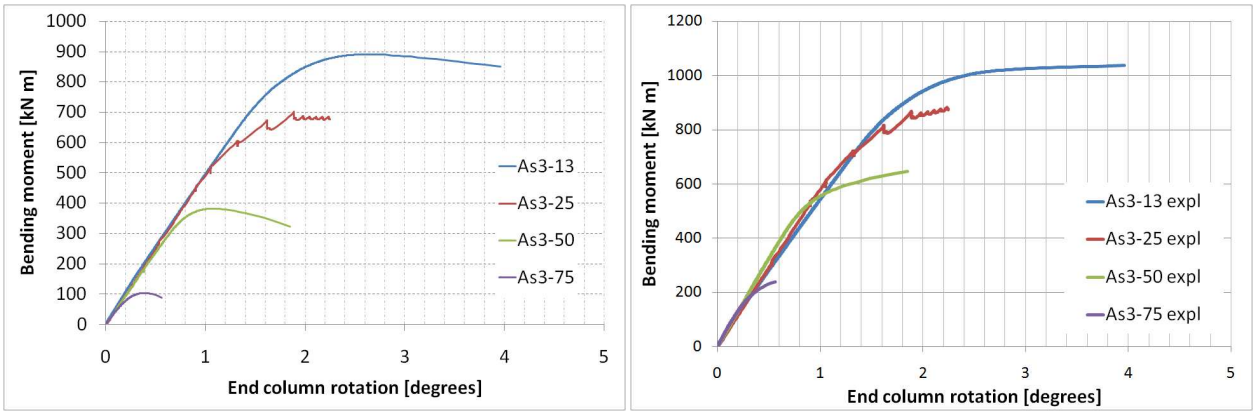

(a) (b)

Figure D6: Short column A combined load tests: moment vs. rotation original curves (a); modified curves with explicit contribution of "codolos"(b).

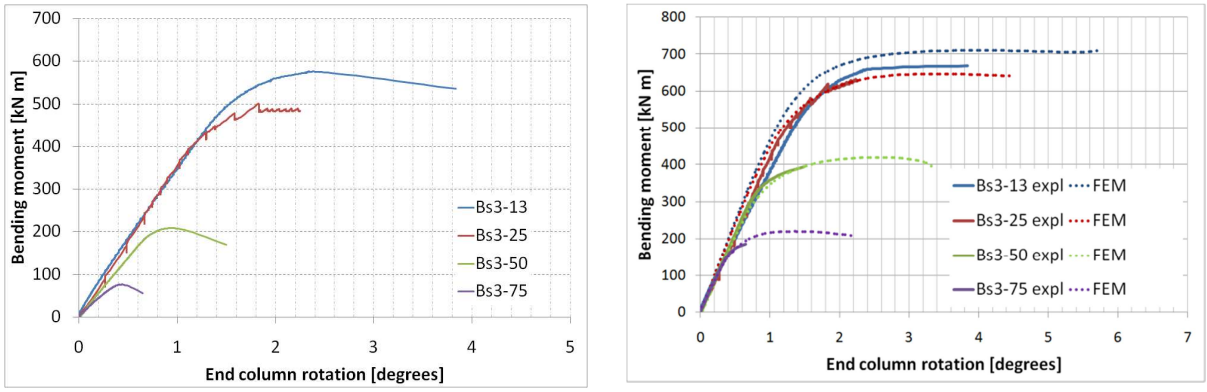

(a) (b)

Figure D7: Short column B combined load tests: moment vs. rotation original curves (a); modified curves with explicit contribution of "codolos"(b).

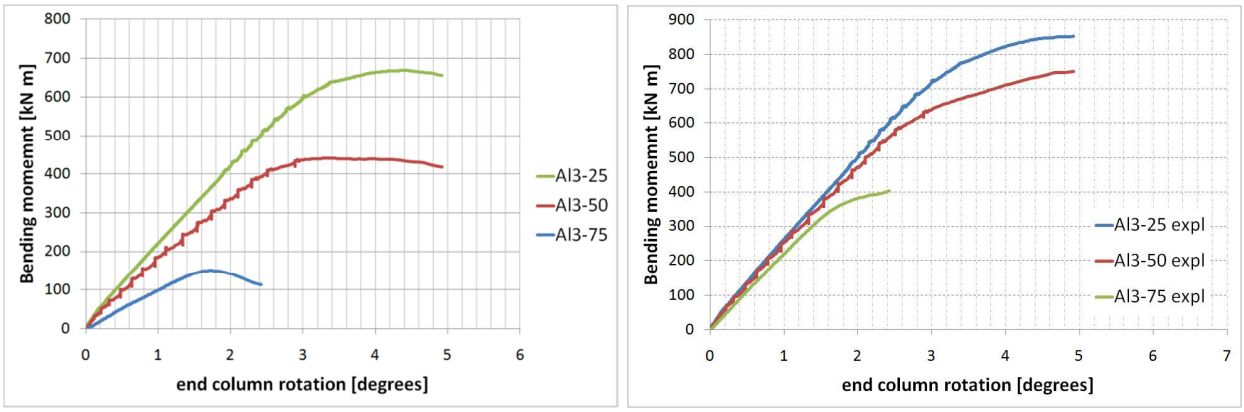

(a) (b)

Figure D8: Long column A combined load tests: moment vs. rotation original curves (a); modified curves with explicit contribution of "codolos"(b).

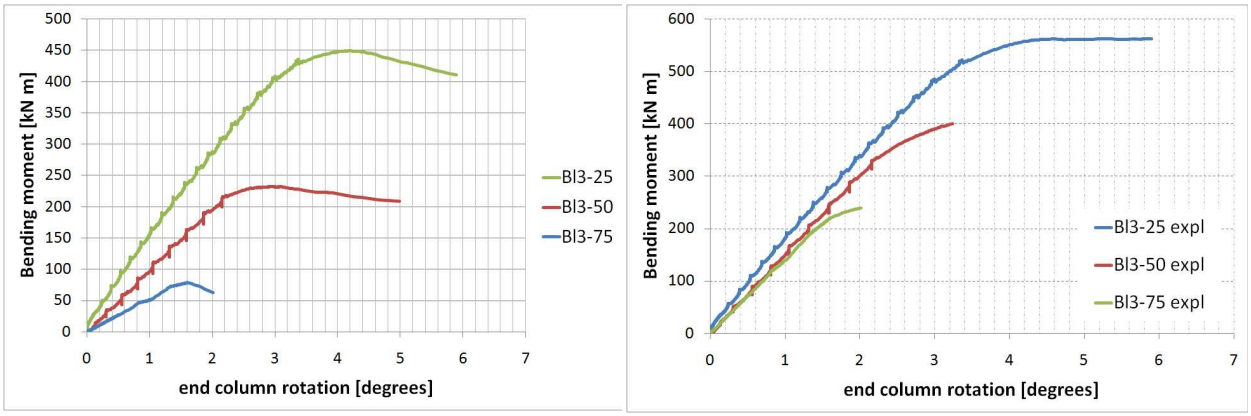

(a) (b)

Figure D9: Long column B combined load tests: moment vs. rotation original curves (a); modified curves with explicit contribution of "codolos"(b).

References

[1] EN1993-1-1:2005. Design of steel structures. Part 1-1: General rules and rules for buildings

[2] EN1993-1-12: Design of steel structures. Part 1-12: Additional rules for the extension of EN1993 up to steel grades S700

[3] EN1993-1-6:2007. Design of steel structures. Part 1-6: Strength and stability of shell structures.

[4] ECCS Publication No. 119. Rules for Member Stability in EN1993-1-1: Background documentation and design guidelines. 2006.